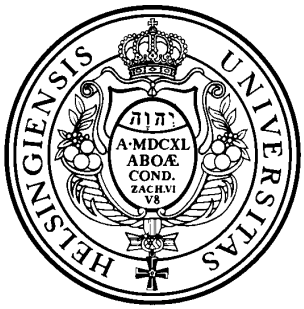

Master's thesis
Physics

MULTIANGULAR SPECTROMETRY AND OPTICAL PROPERTIES OF DEBRIS COVERED SURFACES

Juha Suomalainen

2006

Mentor: Docent Jouni Peltoniemi

Reviewers: Professor Juhani Keinonen and Docent Jouni Peltoniemi

UNIVERSITY OF HELSINKI
DEPARTMENT OF PHYSICAL SCIENCES

P.O. Box 64 (Gustaf Hällströmin katu 2)
00014 University of Helsinki

HELSINGIN YLIOPISTO - HELSINGFORS UNIVERSITET - UNIVERSITY OF HELSINKI

Tiedekunta/Osasto – Fakultet/Sektion – Faculty	Laitos – Institution – Department
Matemaattis-luonnontieteellinen tdk.	Fysiikan laitos

Tekijä – Författare – Author

Juha Suomalainen

Työn nimi – Arbetets titel – Title

Multiangular Spectrometry and Optical Properties of Debris Covered Surfaces

Oppiaine – Läroämne – Subject

Fysiikka

Työn laji – Arbetets art – Level	Aika – Datum – Month and year	Sivumäärä - Sidoantal – Number of pages
Pro Gradu	Syyskuu 2006	57 + 6

Tiivistelmä – Referat – Abstract

Viimevuosina tapahtunut kehitys CCD teknologiassa on vihdoin mahdollistanut myös digitaalisten ilmakuvakameroiden valmistamisen. Digitaalisen kuvauksen käsittelyssä ei ole enää järkevää käyttää manuaalisia filmeille kehitettyjä menetelmiä vaan uusi tekniikka mahdollistaa myös automaattisen tietokoneprosessoinnin. Uusien tehokkaiden datan käsittelytapojen kehittäminen kuitenkin vaatii huomattavaa panostusta kaukokartoituskohteiden valonsironnan perustutkimukseen.

Tämän vuoksi Geodeettisella Laitoksella on kehitetty goniospektrometri FiGIFiGo (*Finnish Geodetic Institute Field Goniospectrometer*), jolla voidaan mitata pienten kaukokartoituskohteiden reflektanssi monisuuntaisesti. Mitattaviksi kohteiksi käyvät esimerkiksi metsän aluskasvillisuus tai asvaltti. FiGIFiGo on helppokäyttöinen ja kannettava laite jonka operoimiseen tarvitaan kaksi ihmistä. Se voidaan koota 15 minuutissa käyttövalmiiksi, jonka jälkeen yhden kohteen sirontaominaisuuksien mittaamiseen kuluu 10 – 30 minuuttia käytetystä tarkkuudesta riippuen. FiGIFiGo:lla voidaan tehdä mittauksia tehokkaasti välillä 400 – 2000 nm sekä ulkona auringonvalolla että sisällä 1000 W laboratorio lampun kanssa. Tässä 'Pro Gradu'-tutkielmassa esitellään FiGIFiGo ja sen mittausten teoreettinen pohja.

Tutkielmassa esitellään myös uusi metodi monesta eri komponentista koostuvan kohteen tutkimiseen. Metodilla voidaan jakaa kohteesta mitattu monisuuntainen reflektanssi sen osien välille, eli esimerkiksi puolukka-jäkälä-kohteesta sironneen valon spektristä voidaan erottaa puolukan osuus. Työssä mittattiin useiden eri keinotekoisten kohteiden reflektanssit ja metodia testattiin soveltamalla sitä näihin tuloksiin. Saadut tulokset vaikuttivat järkeviltä ja ne toivat esille mielenkiintoisia huomioita kohteiden sironnasta. Pienen näytemäärän vuoksi metodin ja tulosten vahvistamiseen tarvitaan vielä lisänäyttöä. Alustavat tulokset vihjaavat kuitenkin että metodi voisi olla hyödyllinen työkalu vastaavien mittausten analysoinnissa

Avainsanat – Nyckelord – Keywords

valon sironta, monisuunta spektrometria, BRF, BRDF, goniospektrometri

Säilytyspaikka – Förvaringställe – Where deposited

Kumpulan tiedekirjasto

Muita tietoja – Övriga uppgifter – Additional information

Tämä Pro Gradu-työ on tehty Geodeettisella Laitoksella.

HELSINGIN YLIOPISTO - HELSINGFORS UNIVERSITET - UNIVERSITY OF HELSINKI

Tiedekunta/Osasto – Fakultet/Sektion – Faculty	Laitos – Institution – Department
Faculty of Science	Department of Physical Sciences

Tekijä – Författare – Author

Juha Suomalainen

Työn nimi – Arbetets titel – Title

Multiangular Spectrometry and Optical Properties of Debris Covered Surfaces

Oppiaine – Läroämne – Subject

Physics

Työn laji – Arbetets art – Level	Aika – Datum – Month and year	Sivumäärä – Sidoantal – Number of pages
Master's thesis	September 2006	57 + 6

Tiivistelmä – Referat – Abstract

Due to the recent development in CCD technology aerial photography is now slowly changing from film to digital cameras. This new aspect in remote sensing allows and requires also new automated analysis methods. Basic research on reflectance properties of natural targets is needed so that computerized processes could be fully utilized.

For this reason an instrument was developed at Finnish Geodetic Institute for measurement of multiangular reflectance of small remote sensing targets e.g. forest understorey or asphalt. *Finnish Geodetic Institute Field Goniospectrometer* (FiGIFiGo) is a portable device that is operated by 1 or 2 persons. It can be reassembled to a new location in 15 minutes and after that a target's multiangular reflectance can be measured in 10 – 30 minutes (with one illumination angle). FiGIFiGo has effective spectral range approximately from 400 nm to 2000 nm. The measurements can be made either outside with sunlight or in laboratory with 1000 W QTH light source. In this thesis FiGIFiGo is introduced and the theoretical basis of such reflectance measurements are discussed.

A new method is introduced for extraction of subcomponent proportions from reflectance of a mixture sample, e.g. for retrieving proportion of lingonberry's reflectance in observation of lingonberry-lichen sample. This method was tested by conducting a series of measurements on reflectance properties of artificial samples. The *component separation method* yielded sound results and brought up interesting aspects in targets' reflectances. The method and the results still need to be verified with further studies, but the preliminary results imply that this method could be a valuable tool in analysis of such mixture samples.

Avainsanat – Nyckelord – Keywords

Light scattering, multiangular, spectrometry, BRF, BRDF, goniospectrometer

Säilytyspaikka – Förvaringställe – Where deposited

Kumpula Science Library

Muita tietoja – Övriga uppgifter – Additional information

The research for this thesis was done at and supported by Finnish Geodetic Institute.

Table of contents

1 PREFACE

This thesis is based on the work and research I have carried through at Department of Remote Sensing and Photogrammetry at Finnish Geodetic Institute between summer 2004 and autumn 2006.

I thank all the personnel at Finnish Geodetic Institute for their help and support at the research work. Especially I thank Jouni Peltoniemi and Sanna Kaasalainen for instructing me in basics of research work and for deepening my understanding in physics of light.

I also want to thank my common-law wife Tiina, my family, and all my friends for their continuous support.

2 INTRODUCTION

Optical remote sensing has traditionally meant taking photographs from an aeroplane with a film camera. After that photographs have been analyzed manually by identifying targets and drawing maps of the heuristic results. Until the very recent years film cameras have been the only option for airborne photography. It is only now that digital CCD based cameras are starting to replace film cameras. Until now scanning analog films has produced all data for computer analysis. Even though film cameras can still provide better spatial resolution, the CCD-cameras have many advantages:

- The data retrieval to computer processable format is more straightforward.
- CCD-cameras can retrieve pixel intensities better than film. Reflectance information can be used in identification of ground targets and for even some target properties analysis.
- The frame rate of digital camera can be many times faster than that of a film camera. The aerial photographs are mostly taken from an aeroplane at movement. By taking multiple successive photographs the same targets can be viewed from multiple viewing angles.
- CCD-cameras provide more freely selectable wavelength channels than film cameras. By selecting optimal wavelength bands the target analysis could be done more accurately. However still at the moment most of the digital cameras use the traditional bands defined by film sensitivity and human eye reception.

Modern digital camera systems can produce such vast amounts of data that it is not economically sensible or even humanly possible to do all analysis manually. Thus automated analysis processes are needed. Simple computerized processes are already in use, but as a general rule the current processes utilize only the same methods as were used already with film cameras. Thus full capabilities of digital aerial photography are not yet unleashed.

In addition to flight cameras optical remote sensing is also made with very similar basis with satellites. Due to limited number of pixels satellites can only provide images either from large areas with very coarse resolution or small areas with good resolution. The coarse resolution images are especially suitable for global monitoring, but on local use their accuracy just is not good enough. Generally spatial resolution of earth observing satellite sensors is between 1 meter and 1 kilometer. Some low-orbit (military) satellites can provide images with almost as fine resolution as flight cameras have, but availability and price of those images are often limiting factors. Satellites always follow their orbits so that wanted places are possible to measure only on certain times. Some satellites have also imaging spectrometers onboard such as, MERIS [1.] on Envisat, and MODIS and MISR [2.] on Terra but unfortunately their spatial resolutions are very modest.

Utilizing the capabilities of digital photography could allow development of completely new remote sensing applications. Aerial photography (with proper atmospheric corrections) can be used to collect the spectral and directional reflectance of the target. With proper georeferencing a Bidirectional Reflectance Factor (BRF

from now on) can be retrieved from concurrent images. Aerial imaging spectrometers such as AISA will probably become more popular in future and enable true hyperspectral measurements in aerial remote sensing. However basic research is still needed even to explore the possibilities of remotely sensed multiangular and multispectral measurements.

The same development of CCD technology that has only now made large format aerial digital cameras possible has also made small and economical spectrometers available. Thus it has become only relatively recently possible to build compact field goniospectrometers, that can be used to retrieve BRF. A goniospectrometer is a basic tool that is very useful for a number of uses in study and development of remote sensing techniques. However still no commercial goniospectrometers are available, but each research group must build their own one. This of course limits their number while remote sensing community could easily employ hundreds of goniospectrometers worldwide. Lack of these devices is unfortunate because remote sensing techniques could benefit greatly if only wide BRF libraries were available.

In addition to good technical solutions, digitalized remote sensing also needs reflectance models for e.g. automated target classification. Realistic reflectance models are complicated to build because of complexity of the targets. In case of forest modelling they are also very hard to validate. Even if the observation data of the forest is available, it is very hard to define the same forest accurately to the model. For example RAMI (Radiative Transfer Model Intercomparison) exercises [3.] addressed this problem by not comparing forest reflectance models with real observations but with each other. While this may help to spot evident errors in models, it does not actually validate them. Thus physical forest models should be combined from smaller submodels that are easier to actually validate. If all subcomponents of a larger model can be validated separately then the combined model has larger probability to be accurate.

One such submodel that is needed is a model for forest understorey. The variation of forest understorey can be huge and its reflectance behaviour is most often far from Lambertian. Typical Finnish conifer forest understory is usually a combination of two to five major species and dozens of minor species. All differently weighed combinations cannot be directly measured. Thus it is important to have a model how to build a BRF of a mixed sample from its component's BRFs. For my knowledge empirical tested models for such purpose do not exist, once again partly because of the lack of goniospectrometers.

The problem of modelling reflectance properties of a inhomogeneous 3D sample is complicated. The first approximation to address this problem could be a demand for the separate components of the sample to stay in separate layers. This may be an adequate approximation in some simple cases e.g. when a layer of lingonberry is growing only on top of a layer of lichen. However even solving this simple scenario accurately can produce problems. The first try in solving reflectance of such mixture could be to measure reflectances of both pure samples; pure lichen and pure lingon and summing a weighted sum over these two. However the real life is not that simple, because:

- the weights of the two components vary over observation direction,
- the lingon casts its shadow over the lichen,
- these shadow show differently from different directions,
- multiple scattering occurs also between the two components,
- multiple scattering occurs differently in different packing densities,
- the lichen underneath lingon may differ from open-air-lingon,
- etc.

A new method for analysis of reflectance properties of such sample was developed. This component separation method for extracting the weights of such a sum is presented in this thesis. Also a series of experiments was performed with artificial samples to validate this method. While this method still does not allow building of new mixed sample BRFs, it can be used in assistance during development of further models

2.1 Personal contribution

This thesis consists of two parts. Chapter 4. introduces Finnish Geodetic Institute Field Goniospectrometer (FiGIFiGo) in which development I have had a major role. Chapter 5. presents the results of a research project I carried through using FiGIFiGo.

In summer 2004, when the Finnish Geodetic Institute first employed me, the field goniospectrometer (later named as FiGIFiGo) was of very simple design. At that moment the device was not yet a working goniospectrometer. Since then almost the whole instrument has been rebuilt and almost every part of it has been replaced with an improved one.

Nowadays FiGIFiGo is a reliable and easy to use measurement instrument. It has a wide variety of assisting sensors and accessories, e.g. pyranometer, inclinometer, digital compass, data acquisition card, hydrogen cell, field base, etc. Currently autoguiding and polarizing optics are being developed. I have extensively contributed in practically all development of the current device. Also the measurement control program Gonio.vi and its predecessor GoniOhjaus have been coded purely by myself.

During the latter half of the year 2005 I carried through a series of measurements using FiGIFiGo. The goal was to find out how BRF of a surface alters when more and more debris covers it. Because multiple types of debris were used, also effects of debris's properties could be analysed. I personally planned and carried through these measurements.

The method presented in chapter 3.4 has been developed by me. Also all data analysis was done with Matlab using numerous self-made functions.

2.2 Other goniospectrometers

Basically any spectrometer can be used as a goniospectrometer if its measurement direction is controlled and defined some way. Small one-axis goniometers are commonly used in molecular chemistry in definition of molecular composition of solutions.

Next are listed and described (Figure 1) some of the most well known automated goniospectrometers that can be used to measure remote sensing targets:

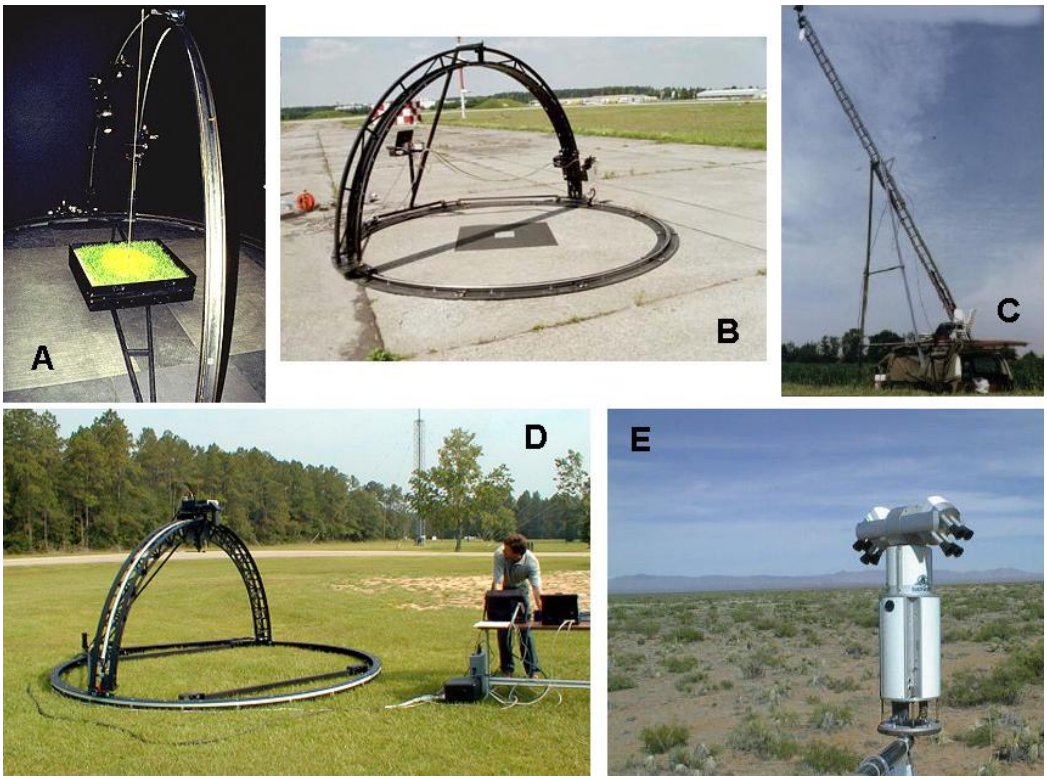

Figure 1. Some other automated goniospectrometers: (A) EGO, (B) FIGOS, (C) MUFSPEM, (D) Sandmeier Field Goniometer, (E) PARABOLA III [10.]

EGO
European Goniometer Facility (EGO) [11.] in European Commission Joint Research Centre, Ispra, Italy, was developed in the mid-90's to be a fully automatic laboratory goniometer. EGO is built with completely different structure than our goniometer making it much sturdier and heavier. Measurement geometry is quite close to our goniometer's with only difference that in EGO the light source is fixed at 2-meter distance from target and it cannot be brought further away. EGO is a laboratory-only-device, which limits its use.

LAGOS/FIGOS
Remote Sensing Laboratories of University of Zurich developed Labor(atory)-Goniometer System (LAGOS) and Field Goniometer System (FIGOS) ([12.] & [13.]) concurrently with EGO. LAGOS and FIGOS is actually the same device with the only difference that in LAGOS an artificial irradiation source is added to FIGOS configuration. Construction of LAGOS is very similar to that of EGO. FIGOS is a fieldworthy device but its portability is still far from ideal.

Sandmeier Field Goniometer (SFG)
In 1998, the Commercial Remote Sensing Verification and Validation (V&V) Team at NASA Stennis Space Center built SFG by reproducing FIGOS and altering it only faintly. They made SFG [14.] slightly lighter and made the sensor head smaller so that smaller phase angles could be measured without shadowing the target.

Mobile Unit for Field SPEctroscopic Measurements (MUFSPEM)
MUFSPEM [15.] by München University of Technology is basically a spectrometer on a 10-meter pole mounted on roof of a tractor or a car. MUFSPEM differs profoundly from FiGIFiGo and the other goniospectrometers introduced above because it is used to measure large targets, e.g. crop fields, from only a few angles.

PARABOLA III
Parabola III [16.] is a spherically scanning radiometer. It does not measure a single target from many directions but measures the irradiation arriving to a single spot from multiple directions. If set over a target, it can be used to determinate the BRDF of a large homogenous sample e.g. forest or field. It is suitable especially for satellite data validation.

ASG (Automated Spectro-Goniometer)
Automated Spectro-Goniometer [17.] by University of California is a small goniospectrometer of rather ingenious design. It consists of two concurrent joints that allow it to observe the target from any direction. Apparently it was originally developed for snow BRDF measurements at field.

In addition to these listed here there exists many morenoteworthy devices, e.g. at University of Utrecht (Neatherlands) and University of Beijing (China), but there is only a little information about them internationally available.

All of these listed devices are practical for their own purposes. MUFSPEM and PARABOLA are suitable for large homogenous targets but they cannot be used in measurement of small samples. EGO, LAGOS, FIGOS, and SFG are fully automated, but none of them are carriable and practically they can be used only on level ground. For practical purposes our FiGIFiGo can match the speed and accuracy of these heavier machines. ASG is also built for field use and it has many good qualities. However its small size restricts sample size and thus demands targets to be quite homogenous. Compared to many of those mentioned earlier, FiGIFiGo lacks automation in white reference measurement and in azimuth angle rotation. Thus human labour is always needed also during the measurements. However at field this is not really an issue because due to unprotected and altering environment human presence is anyway needed. Thus FiGIFiGo can introduce something new for the

goniospectrometer community by being such portable though still high level automated.

FiGIFiGo is only the latest one of Finnish Geodetic Institute's many goniospectrometers. (See Figure 2) The first device was built already in early nineties. FiGIFiGo can be considered to be the 5th model. All the earlier models have been fully manual and remained unnamed. Some of the earlier models were mere prototypes, but especially 3rd model proved to be a good instrument and two refereed articles ([18.] and [19.]) were published with the data collected with it. Closer descriptions of that device can be found from those articles.

Figure 2. Some older manual goniospectrometer models that were developed and used at Finnish Geodetic Institute. Top left picture shows the first model, bottom one shows model 3 and top right one model 4. The operation principle of model 4 is quite similar to our current device, model 5 a.k.a. FiGIFiGo. (Pictures by Jouni Peltoniemi)

3 THEORY

3.1 Short definitions for used terms

In physics of light there are various terms that are used quite loosely. Definitions of terms vary greatly according to the source and exact concept they are used in. All of the terms that are used in various light related applications are not even absolutely defined. The most essential terms that are used in this thesis are defined in the list below.

[Spectral] Irradiance

Irradiance is the amount of radiant power arriving to a surface unit. The SI unit for irradiance is [W/m^2] or [W/m^2/nm]. [4.]

[Spectral] Radiance

Radiance could be described as angular irradiance. It is defined as the amount of radiant power arriving to a surface unit per steradian. The SI unit of radiance is [W/m^2/st] or [W/m^2/st/nm]. [4.]

[Spectral] Total reflectance

Total reflectance (often referred as albedo, simple albedo, or bi-hemispherical reflectance) is defined as the fraction of total incident radiant power upon object that is not absorbed. [4.]

[Spectral] Reflectance Factor

Reflectance has multiple definitions depending on the context. In this thesis reflectance is defined as the proportion between scattered radiances in current illumination/observation conditions from target and from Lambertian scatterer. [4.]

Albedo

The ratio of reflected to incident irradiance is generally defined as albedo and it is thus closely related to reflectance. Albedo of any real surface is a function of wavelength. Albedo has many subdefinitions that are far too often referred only as albedo. Some of these are e.g. single scattering albedo, plane albedo, spherical albedo, geometrical albedo, and bond albedo. [5.]

Bidirectional Reflectance Distribution Function (BRDF)

BRDF of a surface expresses the probability that incident light from one particular direction is reflected to another well-defined direction. [9.] BRDF and BRF is discussed more extensively and more mathematically in section 3.2

Bidirectional Reflectance Factor (BRF)

BRF of a surface expresses the reflectance factor for light coming from one particular direction that is scattered to another well-defined direction. BRDF and BRF is discussed more extensively and more mathematically in section 3.2

Single scattering albedo

Single scattering albedo is defined as the fraction of total incident radiant power upon object that is not absorbed. It is used in radiative transfer as the probability of the interacting photon to scatter forward. What is considered as a single scattering, depends more or less on interpretation. [4.]

Nadir

Nadir is the direction straight down. It is the opposite of zenith, but these terms are often used meaning same thing.

Principal plane

Principal plane is the plane in which the illumination source, the target, and the nadir of the target are.

Forward scattering

Forward scattering is an event where light is scattered to the other side of nadir than the light source is. I.e. the difference in azimuth angles of incoming and leaving rays is greater than 90^{o}. (See description of the angles in Figure 3 on page 11)

Backward scattering or *backscattering*

Backward scattering is opposite of forward scattering.

Forward/backward scatterer

Forward scatterer is a target that scatters considerably more to the forward scattering direction than to the backward scattering direction. Backward scatterer or backscatterer is of course opposite of forward scatterer.

Lambertian surface

A surface that reflects irradiance upon it according to Lambert's cosine law, i.e., reflected radiance is directly proportional to the cosine of the zenith angle from which it is viewed. In practice a Lambertian has reflectance, which does not depend on the viewing angle.[5.]

Diffuse illumination

Diffuse illumination is the portion of illumination that does not come from the direction of primary light source. E.g. blue sky and reflections from clouds.

3.2 BRF and BRDF

Bidirectional Reflectance Factor (BRF from now on) is a function or a set of data that produces the reflectance factor of a target as function of the illumination and observation geometry. Bidirectional Reflectance Distribution Function (BRDF) is closely related to BRF. It expresses the probability of incident ray from specific direction to scatter to defined space angle. Bidirectional in both of these refers to the directions of incidence (***i***) and observation (***o***). Most often both of these directions are defined with an azimuth (θ) and a zenith (ϕ) angle. (See Figure 3)

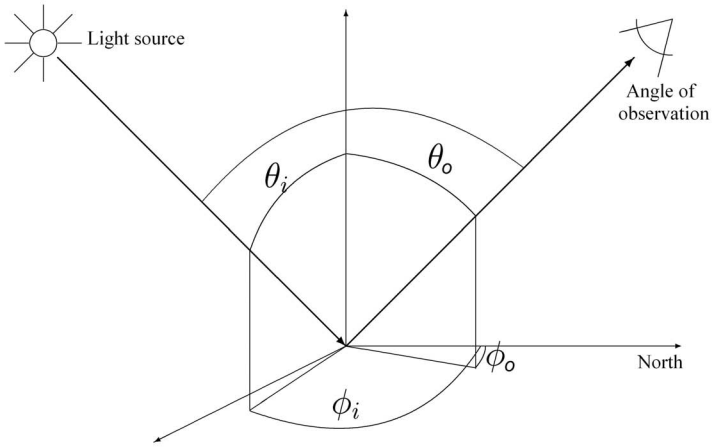

Figure 3. Geometry of BRDF measurement. Directions of incidence and observation are defined by two angles each. θ_i and θ_o are incidence and observation zenith angles. ϕ_i and ϕ_o are azimuth angles respectively. [18.]

Practically all reflectance related quantities that mentioned in this thesis, e.g. reflectances, albedos, radiances, and irradiances, are wavelength dependent. However, due to size and readability reasons, $(\ldots, \lambda)$ is left out from equations. Also directions incidence and observation are repeated continuously, thus most often abbreviations $\boldsymbol{i} = (\theta_i, \phi_i)$ and $\boldsymbol{o} = (\theta_o, \phi_o)$ are used. I.e while $R(\theta_i, \phi_i; \theta_o, \phi_o; \lambda)$ would be more precise and accurate expression for reflectance, it is referred only as $R(\boldsymbol{i}, \boldsymbol{o})$.

3.2.1 Derivation of BRDF and BRF

[4.], [5.], and [6.]

Bidirectional Reflectance Distribution Function (BRDF) is a property of a surface (or a particle) that expresses the probability per unit solid angle of a photon coming from one direction to scatter to another well-defined direction. BRDF has units of [sr^{-1}]. If the solid angles of incidence and observation are infinitesimally small, BRDF (f) is defined as:

$$f(\mathbf{i},\mathbf{o}) = \frac{dL_{\text{Target}}(\mathbf{i},\mathbf{o})}{dE_i(\mathbf{i})} \tag{1}$$

where ***i*** and ***o*** are respectively the directions of incidence and observation, dL_{Target} is the reflected radiance per unit solid angle, and dE_i is the incident irradiance per unit solid angle. In theoretical use BRDF is very useful concept, but it has some drawbacks for practical applications. Thus two simplifications are made for the definition of Bidirectional Reflectance Factor (BRF). First both solid angles are increased to contain measurable quantities of energy. Secondly, instead of hard-to-measure irradiance at target surface, the radiance from Lambertian surface is used as reference. BRF (R) is defined as:

$$R(\mathbf{i},\mathbf{o}) = \frac{L_{\text{Target}}(\mathbf{i},\mathbf{o})}{L_{\text{Lambertian}}(\mathbf{i},\mathbf{o})} \tag{2}$$

where L_{Target} is reflected radiance from the target surface and $L_{\text{Lambertian}}$ is similarly measured radiance from perfect Lambertian reference panel. Thus BRF is unit-less. Because perfect Lambertian surfaces are impossible to produce, in practical use a correction term (k) is added. Also, because reference radiance is assumed to be isotropic by definition, the reference may be measured from different direction (***o´***) than the target.

$$R(\mathbf{i},\mathbf{o}) = \frac{L_{\text{Target}}(\mathbf{i},\mathbf{o})}{L_{\text{Reference}}(\mathbf{i},\mathbf{o}')} k(\mathbf{i},\mathbf{o}') \tag{3}$$

For a good white reference panel (e.g. Spectralon, see Appendix A), the correction term is very close to 1.

Let us next derive the relation between BRF and BRDF. By definition irradiance E and radiance L are connected via:

$$E = \int_0^{2\pi}\int_0^{\pi} L(\theta,\phi)\cos\theta\sin\theta\, d\theta\, d\phi \tag{4}$$

By denoting $\mu = cos(\theta)$, equation (4) can be written as:

$$E = \int_0^{2\pi}\int_0^{1} L(\theta,\phi)\,\mu\, d\mu\, d\phi \tag{5}$$

If the scatterer is Lambertian (i.e. $L \neq L(\theta, \phi)$) the integral can be solved implicitly:

$$E = \pi L_{\text{Lambertian}} \tag{6}$$

So by combining equations (2) and (6), BRF can be written as:

$$R(\mathbf{i},\mathbf{o}) = \pi \frac{L_{\text{Target}}(\mathbf{i},\mathbf{o})}{E_{\text{r Lambertian}}(\mathbf{i},\mathbf{o})} \tag{7}$$

Because the reference panel is assumed to be Lambertian, incident and reflected irradiances are equal. I.e. $E_{\text{r Lambertian}} = E_i$. If incidence and observation solid angles are infinitesimally small or the target is an isotropic scatterer, then BRF can further written as:

$$R(\mathbf{i},\mathbf{o}) = \pi \frac{dL_{\text{Target}}(\mathbf{i},\mathbf{o})}{dE_{\text{i}}(\mathbf{i},\mathbf{o})} \tag{8}$$

from which BRDF, as presented in equation (1), can be extracted, resulting to a handy relation between BRF and BRDF:

$$R(\mathbf{i},\mathbf{o}) = \pi\, f(\mathbf{i},\mathbf{o}) \tag{9}$$

In practice BRF behaves as an angular average of BRDF. Thus, if sharp, sub-resolution angular effects are not expected, equation (9) can be quite safely implemented to BRF of any natural surface.

3.2.2 BRF retrieval in natural illumination

On a clear day in natural sunlight illumination most of the light to target comes directly from sun. However, due to scattering from atmosphere and surroundings, the target is also illuminated from all other directions too. This hemispherical portion of illumination is referred as *diffuse irradiation*.

To be exact, even the direct irradiation is not exactly parallel. Due to the size of sun's disc, the direct light has angular diversity of approximately 0.5°. This diversity is so small that in most practical cases the sunlight can be considered to be parallel. However this is not the case in study of hot spot effect, where very sharp effects are observed. This diversity also sets the minimum resolution of BRF that is theoretically possible to measure using sunlight. Technical restrictions, e.g. size of the footprint, optics diameter, and measurement distance, set the resolution even higher.

In it's most ideal case, the diffuse light is the irradiance of the blue sky. In real life situations surrounding trees, buildings, scientists, instrumentation, clouds, and rest of the atmosphere all have some effect in diffuse light, either by reflecting more of it or blocking the scatterer that is further away. Our prior measurements have showed that on an open ground with only a little or no clouds in the sky the diffuse illumination is fairly isotropic. Due to Rayleigh scattering in atmosphere the diffuse light is generally the more intense the shorter the wavelength is (blue sky). At ultraviolet and blue wavelengths portion of diffuse light may be up to one half, while usually on longer wavelengths the natural diffuse light presents only less than 10% of illumination.

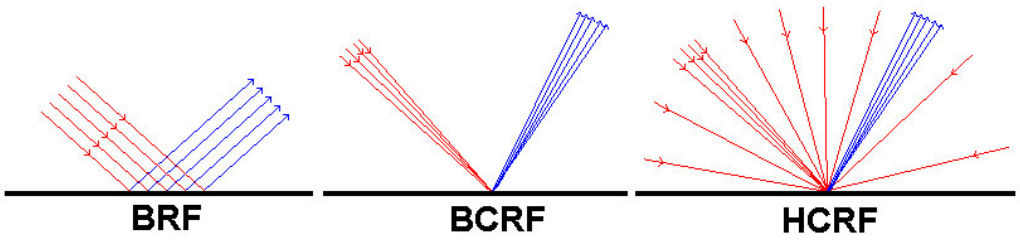

Figure 4. Geometries of Bidirectional Reflectance Factor (BRF), Biconical Reflectance Factor (BCRF), and Hemispherical Conical Reflectance Factor (HCRF). BRF is the most theoretical factor of these three. Most scattering models require and/or produce BRF. Laboratory measurements produce BCRF and sunlight measurements produce HCRF. Transfer functions are needed to combine different measurements and theories.

The illumination and observation geometry in real measurements is more complicated than one would first come to think. What is actually measured with a goniospectrometer is not Bidirectional Reflectance Factor (BRF) but in sunlight measurements Hemispherical Conical Reflectance Factor (HCRF) and in laboratory measurements Biconical Reflectance Factor (BCRF). (Figure 4) [8.]

Let us next derive the retrieval of BRF from data measured in natural illumination. If the intensity of incident radiation is assumed to be spatially constant, the radiance from point (x_0, y_0) at the target to direction $\boldsymbol{o}$ with an arbitrary incident radiance is:

$$L_o'(\mathbf{o}, x_0, y_0) = \iint_{2\pi} \frac{\partial R(\mathbf{i}', \mathbf{o}, x_0, y_0) L_i(\mathbf{i}')}{\partial \Omega_i'} d\Omega_i' \tag{10}$$

where R is the BRF of the target at point (x_0, y_0), L_i is the incident radiance as function of direction, Ω_i' is the solid angle incoming radiance, and the integral is over the whole hemisphere. If the target is inhomogeneous BRF is a function of location. Incident illumination in equation (10) can still be divided between direct and diffuse illumination. If direct sun irradiance is assumed to be from infinitely small and distant source at direction Ω_i, then the previous equation can be derived to form:

$$L_o'(\mathbf{i}, \mathbf{o}, x_0, y_0) = R(\mathbf{i}, \mathbf{o}, x_0, y_0) L_{\text{Direct}} + \iint_{2\pi} \frac{\partial R(\mathbf{i}', \mathbf{o}, x_0, y_0) L_{\text{Diffuse}}(\mathbf{i}')}{\partial \Omega_i'} d\Omega_i' \tag{11}$$

where L_{Direct} and $L_{Diffuse}$ are the incident irradiances. The actual observed intensity L_o can be calculated by integrating the previous equation over the solid angle of sensor head and over the surface area of observation footprint:

$$L_o(\mathbf{i}, \mathbf{o}) = \iint_{\text{Footprint}} \frac{\partial}{\partial x \partial y} \left(\iint_{\text{Sensor}} \frac{\partial L_o'(\mathbf{i}, \mathbf{o}', x, y)}{\partial \Omega_o'} d\Omega_o' \right) dx dy \tag{12}$$

where Ω_o is a function of x and y (and z). If observing optics occupy only a small solid angle and the footprint size is small compared to distance of observation, combination of equations (11) and (12) can be approximated to be:

$$L_o(\mathbf{i},\mathbf{o}) = R(\mathbf{i},\mathbf{o})L_{\text{Direct}} + L_{\text{Obs.Shaded Target}}(\mathbf{i}) \tag{13}$$

where $L_{Obs.\ Shaded\ Target}$ is measured intensity of radiation from shadowed target and R is the effective BRF of whole target. Our prior measurements have showed that $L_{Obs\ Shaded\ Target}$ is not significantly a function of observation angle, but it depends especially on the zenith angle of sun position. This is logical perception, because the diffuse illumination is arriving fairly isotropically from all directions, but total irradiation depends on the zenith angle.

It is now easy to extract the BRF from equation (13):

$$R(\mathbf{i},\mathbf{o}) = \frac{L_{\text{Obs. Target}}(\mathbf{i},\mathbf{o}) - L_{\text{Obs.Shaded Target}}(\mathbf{i})}{L_{\text{Direct}}(\mathbf{i})} \tag{14}$$

It is known that for an ideal white reference panel $R = 1$, and especially $R(Nadir\ Observation) = 1$. Thus the intensity of direct irradiation can be solved by adapting equation (13) to measurement of reference panel:

$$\begin{aligned} L_{\text{Direct}}(\mathbf{i}) &= \frac{L_{\text{Obs. Reference}}(\mathbf{i}, Nadir) - L_{\text{Obs.Shaded Reference}}(\mathbf{i}, Nadir)}{R_{\text{Reference}}(\mathbf{i}, Nadir)} \\ &= L_{\text{Obs. Reference}}(\mathbf{i}, Nadir) - L_{\text{Obs.Shaded Reference}}(\mathbf{i}, Nadir) \end{aligned} \tag{15}$$

By combining equations (14) and (15):

$$R(\mathbf{i},\mathbf{o}) = \frac{L_{\text{Obs. Target}}(\mathbf{i},\mathbf{o}) - L_{\text{Obs.Shaded Target}}(\mathbf{i})}{L_{\text{Obs. Reference}}(\mathbf{i}, Nadir) - L_{\text{Obs.Shaded Reference}}(\mathbf{i}, Nadir)} \tag{16}$$

These irradiances can directly be transformed to intensities (I) measured by spectrometer if configuration of optics is not varied in between. So finally an equation for BRF containing only measurable quantities is formed:

$$R(\mathbf{i},\mathbf{o}) = \frac{I_{\text{Obs. Target}}(\mathbf{i},\mathbf{o}) - I_{\text{Obs.Shaded Target}}(\mathbf{i})}{I_{\text{Obs. Reference}}(\mathbf{i}, Nadir) - I_{\text{Obs.Shaded Reference}}(\mathbf{i}, Nadir)} \tag{17}$$

where, once again, all quantities are functions of wavelength.

3.2.3 Pyranometer correction

At field there is almost always some variance in intensity of illumination during the typical BRF retrieval time of 20 minutes. This is caused by the water vapour in atmosphere, and by the movement of the sun. During the measurements a

pyranometer is used to monitor and record the incident irradiance. For each measured intensity the following correction is applied:

$$I' = \frac{I(\mathrm{t})}{P_{Total}(\mathrm{t})} \tag{18}$$

The reflected intensity $I(t)$ is divided by the total incident irradiance $P_{Total}(t)$. Both values have been measured simultaneously at time t. As the first approximation the same correction may be used for both shaded and fully illuminated measurements. However it may be that the atmospheric effect that causes the alteration in direct illumination may have no effect or even an opposite effect in amount of diffuse light. A better correction could be obtained by measuring separately the diffuse incident irradiance and by correcting the intensities of shaded measurements with:

$$I''_{Shaded} = \frac{P_{Diffuse}(\mathrm{t}_0)}{P_{Total}(\mathrm{t}_0)} \frac{I_{Shaded}(\mathrm{t}_0)}{P_{Diffuse}(\mathrm{t})} \tag{19}$$

where $P_{Diffuse}(t_0)$, and $P_{Total}(t_0)$ are the diffuse incident irradiance, total incident irradiance. $I_{Shaded}(t_0)$ is the intensity from target that has been shadowed from direct incident light.

However the current configuration of FiGIFiGo contains only one pyranometer so the complete equation used for retrieval of BRF is received by combining equations (16) and (18):

$$R(\mathbf{i},\mathbf{o}) = \frac{\frac{I_{\mathrm{Target}}(\mathbf{i},\mathbf{o},t_{\mathrm{Target}})}{P_{Total}(t_{\mathrm{Target}})} - \frac{I_{\mathrm{Shaded\ Target}}(\mathbf{i},t_{\mathrm{Shaded\ Target}})}{P_{Total}(t_{\mathrm{Shaded\ Target}})}}{\frac{I_{\mathrm{Reference}}(\mathbf{i},Nadir,t_{\mathrm{Reference}})}{P_{Total}(t_{\mathrm{Reference}})} - \frac{I_{\mathrm{Shaded\ Reference}}(\mathbf{i},Nadir,t_{\mathrm{Shaded\ Reference}})}{P_{Total}(t_{\mathrm{Shaded\ Reference}})}} \tag{20}$$

If an additional diffuse light pyranometer were installed, the BRF with better diffuse light correction could be obtained by combining equations (16) and (19):

$$R(\mathbf{i},\mathbf{o}) = \frac{\frac{I_{\mathrm{Target}}(\mathbf{i},\mathbf{o},t_{\mathrm{Target}})}{P_{Total}(t_{\mathrm{Target}})} - \frac{P_{Diffuse}(t_{\mathrm{Shaded\ Target}})}{P_{Total}(t_{\mathrm{Shaded\ Target}})} \frac{I_{\mathrm{Shaded\ Target}}(\mathbf{i},t_{\mathrm{Shaded\ Target}})}{P_{Diffuse}(t_{\mathrm{Target}})}}{\frac{I_{\mathrm{Reference}}(\mathbf{i},Nadir,t_{\mathrm{Reference}})}{P_{Total}(t_{\mathrm{Reference}})} - \frac{P_{Diffuse}(t_{\mathrm{Shaded\ Reference}})}{P_{Total}(t_{\mathrm{Shaded\ Reference}})} \frac{I_{\mathrm{Shaded\ Reference}}(\mathbf{i},Nadir,t_{\mathrm{Shaded\ Reference}})}{P_{Diffuse}(t_{\mathrm{Reference}})}} \tag{21}$$

3.2.4 BRF retrieval in laboratory illumination

In laboratory measurements illumination is produced with a high power lamp. Most of the measurement process and data analysis is done quite similarly as at field but only with some simplifications. E.g. due to the stability of light source and non-existence of diffuse light, pyranometer and diffuse light correction can be ignored. Laboratory and sun illumination however have some profound differences. Next there are listed the pros and cons of using laboratory light compared to natural illumination.

Pros in laboratory illumination:

- Irradiance is more time-stable
- Direction of illumination is constant and can be selected
- No diffuse light. BRF and BRDF can be retrieved reliably.
- No atmospheric absorbance, i.e. no completely dark wavelengths in the middle of the spectrum
- Possibility to measure does not depend on weather or time.

Cons in laboratory illumination:

- Irradiance is generally smaller than with sun i.e. more white noise,
- Spectrum of lamplight is different than that of sunlight. All wavelengths that are observed in sunlight cannot be measured in laboratory.
- Irradiance is not spatially constant because of:
    i. Uneven spot caused by finite sized filament and imperfectness of the optics of the lamp
    ii. The lamp is quite close to target. Thus $1/R^2$ weakening of irradiance has significant effect
- Variance of incident direction is larger. That is because the phase angle of lamp's reflector is typically larger than sun's disc and direction of incident irradiance varies spatially.
- No natural diffuse light. Thus applying results back to remotely sensed measurements is not that straightforward.

Despite of its cons, laboratory measurements provide a good alternative to field measurement. Field measurements are most suitable for practical remote sensing needs where results are compared directly with remotely sensed data, and for targets that cannot be moved. Laboratory measurements are generally better for more theoretical studies, where true BRF/BRDF is requested and full control over the measurement is wanted.

3.3 Light scattering effects

3.3.1 Basic reflection processes

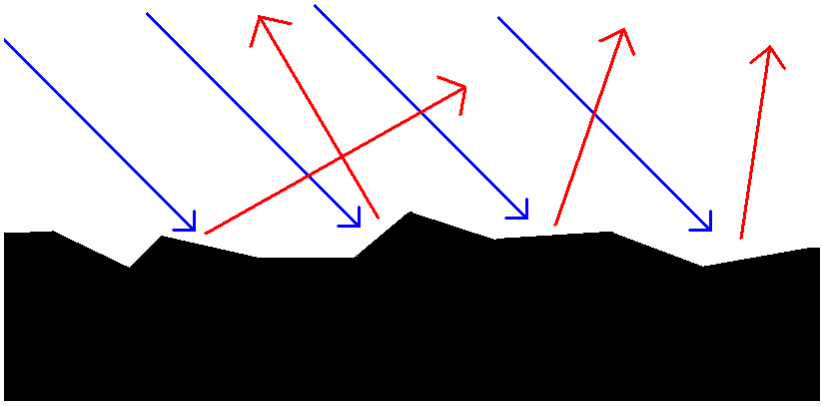

Figure 5. Specular reflections from a rough surface. The surface may be apparently flat for human eye and touch, but have significant roughness on wavelength scale,

The classical example of specular reflection is a reflection from a flat mirror. However so that specular reflection should happen, the surface does not need to be flat or reflecting for human observation. Specular reflection happens on any surface that has flatness on the wavelength scale, and also regardless of the horizontality of the surface. A great portion of so-called diffusely reflected light is scattered through specular reflection from tilted mini-surfaces on the macroscopic surface. (Figure 5) While specular reflection from naturally rough surface may produce nearly diffuse light, it usually emphasizes forward scattering. This is due to the fact that in a horizontally flat surface the mini-surfaces are still horizontal on average. Thus specular reflection is often spread to wider set of angles around the "real specular direction". On somehow organized surfaces, such as vegetation or man-made surfaces, the assumption of average horizontality may not always be true, but it is usually a good first approximation.

However while specular reflection is an important mechanism for reflection from hard surfaces, it is not the only one. On scattering from non-metallic substances a part of the incident light always enters the substance. The light inside the medium goes through one or more of the following processes: [5.]

- Light may be absorbed. Absorption is very wavelength dependant process and this is the main reason why different substances seem to have different colours.
- Light transmits its way through the particle to direction defined by the particle shape and refraction index. Happens most clearly in diamonds and other clear crystals.
- Light may volume-scatter inside the medium similarly as happens in clouds.

The weighing between surface reflections and inside medium scattering depends always on the target and wavelength.

3.3.2 The hot spot effect

[20.]

It is well known that near the direct backscattering angle (direction where incident and reflected light are travelling exactly opposite directions) reflectance factor is significantly higher than closely around it. This can be seen e.g. from aeroplane as a bright spot (i.e. hot spot) where aeroplane's shadow should be. This sudden brightening has two separate sources.

The earlier explanation, called *mutual shadowing* or *shadow hiding*, was first introduced at late 19th century. German astronomer Hugo von Seeliger found out how brightness of Saturn's rings varied significantly depending on the positions of Sun, Earth, and Saturn. Always when Saturn was in opposition it's rings became significantly brighter. This was explained with mutual shadowing.

Mutual shadowing is an effect where loosely packed particles cast shadows over each other. If the medium is observed from any other direction than that of illumination some shadowed areas are seen. In direct backscattering direction no shadows are seen and thus medium seems to be brighter.

The modern quantum physics have introduced also a second additional explanation to the effect. Amplification by *coherent backscatter* is caused by interaction of multiply reflected photons. When an incident photon reflects from the medium it can have one or more reflections. When multiple collisions occur the light follows a certain path inside the medium. However, because all light reflection processes are reversible, the same path can pass photons both directions. The incident wave front (photon) can travel through the path both ways. In the case of a retro reflection, the both parts of the front are heading to same direction and are in exactly same phase. Waves in same phase strengthen each other thus producing brighter reflectance in backscattering direction.

Both shadow hiding and coherent backscatter are usually present in hot spot effect. Shadow hiding is an effect of single scattering while coherent backscatter occurs only in case of multiple scattering. Thus shadow hiding is usually the leading effect in dark mediums, where absorption reduces chance of multiple scattering. Generally coherent backscatter produces narrower hot spot peaks than shadow hiding.

3.3.3 BRF shapes

[18.] and [19.]

BRFs can come in many different shapes. Shape of BRF stands here for shape of reflectance as function of observation angle in three-dimensional plot. (See Figure 6) BRF shape is caused by macroscopic geometry of target and reflectance properties of surfaces and particles.

According to radiative transfer model, BRDF of homogenous medium where occurs only single scattering follows Lommel-Seeliger law: [6.]

$$f_R = \frac{\varpi_0}{4\pi} \frac{1}{\mu_r + \mu_i} \tag{22}$$

where ϖ_0 is the single scattering albedo of the particles in the medium, μ_i and μ_r are cosines of incident and reflection zenith angles. Simple 1D radiative transfer model does not natively take specular reflection, multiple scattering, inhomogeneous mediums, shadow hiding, or coherent backscatter in to account. Thus Lommel-Seeliger law alone is not a good enough model to express BRDFs of real natural surfaces. However Lommel-Seeliger gives a good estimate for what kind of BRF shapes are found.

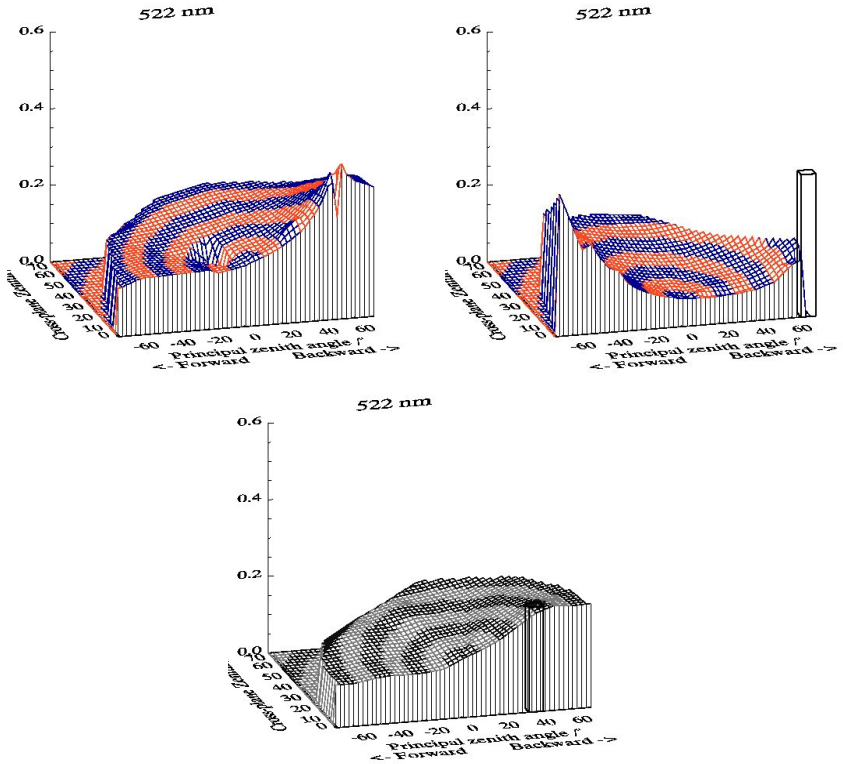

Figure 6. Typical measured BRF shapes with a single incident illumination direction. BRFs here are presented in cylindrical coordinates. Z-axis is reflectance factor, in-plane distance from center is zenith angle, and rotation is azimuth angle. Lichen (top left) is a strong backscatterer, moss (top right) is forward scatterer but has also concave shape, and gravel (bottom) is flattish. (Figures by Jouni Peltoniemi)

Unfortunately there is no easy universal way to express mathematically all BRF shapes that occur in natural targets. The observed BRF is a sum of multiple interacting mechanisms, which effect cannot be modelled easily. Thus only typical BRF features can be listed.

- Often BRF is of concave shape. (See Figure 6), Thus quite often the reflectance factor has a minimum at or near at nadir observation angle.
- Often BRF is weighed either on forward or backward direction
- The most characteristic effects occur usually on the principal plane.
- Hot spot effect occurs always, but often the peak is so thin that it is not observed because of the observer's own shadow.

3.4 Separating reflectance spectrum components

[21.]

I developed myself the method presented in this chapter for separating impact of target's subcomponent in reflectance spectrum. Retrospectively it came to my knowledge that quite similar method, known as *linear spectral unmixing*, is already in use with satellite image processing. [22.] Both of these methods are based on the same idea of extracting reference spectrum shapes from measured spectrum. Such methods make it possible to extract spatially sub-resolution components from an pixel and find their proportions.

In satellite image analysis most often pure pixels (e.g. pure forest pixel, or asphalt pixel) are selected from same satellite image and their proportions are extracted from mixed pixels. In my study BRFs of pure samples are measured separately and they are further separated down to single and multiple scattered components with aid of multiangular information. Knowledge of single scattered component spectrum shape allows more precise and more physical approach to be used in unmixing method. This advanced approach is not included in basic linear spectral unmixing method.

3.4.1 Separating single scattered component

A simple model was created for the scattering from a homogenous medium. The following assumptions were used:

1. The medium consists of particles with single scattering albedo *a*
2. Albedo depends on wavelength but does not depend on angle of incidence (or scattering).
3. An incident ray may or may not scatter multiple within medium After each collision the ray has probability, *t*, to scatter out of the medium.
4. *t* depends only on geometrical factors and thus it is function of only scattering angle.

By calculating the probability for a ray not to be absorbed, a simple relation for reflectance *R* is acquired:

$$R(\theta,\lambda) = 1 - a(\lambda)\sum_{n=1}^{\infty}\left[(1-a(\lambda))(1-t)\right]^{n} = 1 - \frac{a(\lambda)}{a(\lambda) + t\,(1-a(\lambda))} \tag{23}$$

Because the probability for the ray to scatter out from medium is different to different angles, is the out-scattering probability *t* treated as function of scattering angle $t(\theta)$. While this not a physical way to do it, it is an effectiveway to add angular dependency to the model and if high order multiple scattering does not have significant role in scattering it does not compromise too much accuracy.

If out-scattering probability $t(\theta_0)$ is known or can be intuitively guessed for one angle θ_0 and $R(\theta_0, \lambda)$ is known for all wavelengths, albedo can be easily inverted from equation (23):

$$a(\lambda) = \frac{t(\theta_0)(1 - R_{Tot}(\theta_0, \lambda))}{1 - (1 - t(\theta_0))(1 - R_{Tot}(\theta_0, \lambda))} \tag{24}$$

Similarly angle dependence of t can be solved if $R_{Tot}(\theta, \lambda_0)$ and $a(\lambda_0)$ are known.

$$t(\theta_0) = \frac{a(\lambda_0)R_{Tot}(\theta, \lambda_0)}{(1 - a(\lambda_0))(1 - R_{Tot}(\theta, \lambda_0))} \tag{25}$$

Now that $a(\lambda)$ and $t(\theta)$ are defined can an estimate for reflectance caused by single scattering r_{Single} be calculated with:

$$r_{Single}^{Theory}(\theta, \lambda) = t(\theta)(1 - a(\lambda)) \tag{26}$$

By fitting functions (24), (25), and (26) to measured multi-angular data set can $a(\lambda)$ and $t(\theta)$ be solved. Because of the rough approximations this model cannot be perfect and the estimated total reflectances probably do not fit perfectly. Thus single scattering reflectance should be used with correction term.

$$r_{Single}(\theta, \lambda) = \frac{R^{Measured}(\theta, \lambda)}{R^{Theory}(\theta, \lambda)} r_{Single}^{Theory}(\theta, \lambda) \tag{27}$$

The final equation for single scattered reflectance component can be formed by combining equations (23), (26), and (27):

$$r_{Single}(\theta, \lambda) = [t(\theta) + a(\lambda) - t(\theta)a(\lambda)]R^{Measured}(\theta, \lambda) \tag{28}$$

3.4.2 Derivation of multiple scattered components

As hinted earlier the task here is to observe a target that consists of two components. E.g. a case of lingonberry bushes on lichen. The component forming the solid layer on bottom is referred here as ‘base’ and the other one forming a layer above the base is referred as debris. I.e. lingon is the debris and lichen is the base.

Let us start observing the reflectance from such a target by examining rays’ scattering paths. Each ray scattered from debris-base-mixture sample has travelled through an individualistic path that consists of a certain number of single scatterings from base (N_{Base}) and a certain number of single scatterings from debris (N_{Debris}). If all single scatterings from a component can be assumed to be identical, then the path can be effectively described with only 2 variables N_{Base} and N_{Debris}.

Let us also assume that reflectance spectrum of single scattered light is not a function of scattering angle, i.e. wavelength of light does not have an effect on scattering

angle. Thus reflectance spectrum r produced by a path with N_{Base} and N_{Debris} scatterings from each component is:

$$r_{N_{Base},N_{Debris}} = c_{N_{Base},N_{Debris}}(\mathbf{i},\mathbf{o}) \cdot a_{Base}^{N_{Base}}(\lambda) \cdot a_{Debris}^{N_{Debris}}(\lambda) \tag{29}$$

where a_{Base} and a_{Debris} are single scattering albedos and c is an variable describing probability of the path so that:

$$R(\lambda,\mathbf{i},\mathbf{o}) = \sum_{N_{Base}} \sum_{N_{Debris}} r_{N_{Base},N_{Debris}}(\lambda,\mathbf{i},\mathbf{o}) \tag{30}$$

According to equation (29) the single scattering components are:

$$\begin{aligned} r_{SingleBase} &= r_{1,0} = c_{1,0}(\mathbf{i},\mathbf{o}) \cdot a_{Base}(\lambda) \\ r_{SingleDebris} &= r_{0,1} = c_{0,1}(\mathbf{i},\mathbf{o}) \cdot a_{Debris}(\lambda) \end{aligned} \tag{31}$$

It is noteworthy that c is not a function of wavelength. Thus the shape of the spectrum of all other paths can be calculated from spectra of single scatterings from base and debris.

$$r_{N_{Base},N_{Debris}}(\lambda,\mathbf{i},\mathbf{o}) = c'_{N_{Base},N_{Debris}}(\mathbf{i},\mathbf{o}) \cdot r_{SingleBase}^{N_{Base}}(\lambda,\mathbf{i},\mathbf{o}) \cdot r_{SingleDebris}^{N_{Debris}}(\lambda,\mathbf{i},\mathbf{o}) \tag{32}$$

Thus each path leaves its own spectral signature in scattered light that cannot be summed from the other ones, or as it can be expressed mathematically: spectra of paths are orthogonal.

3.4.3 Separating scattering paths from a mixed sample spectrum

Let's assume that we have measured a spectrum $\boldsymbol{r}_{Mixed}$ of a target that is a combination of two components: base and debris. The shapes of single scattering reflectance spectra $\boldsymbol{r}_{SingleBase}$ and $\boldsymbol{r}_{SingleDebris}$ are known at same geometry as the measurement was made. Each spectrum is organized as a row vector with wavelength as index:

$$\mathbf{r}_i = \left[r_i(\lambda_1), \quad r_i(\lambda_2), \quad \ldots \quad r_i(\lambda_n) \right] \tag{33}$$

Let us assume that both debris and base have single scattering albedos that are significantly smaller than 1. Thus multiple scattering dies off quickly and number of significant scattering paths is finite and well defined. E.g. if two scattering is assumed to be enough the list of paths would be:

1. Two scatterings from base but none from debris
2. Single scattering from base
3. Single scattering from both base and debris
4. Single scattering from debris
5. Two scatterings from debris but none from base

In order to identify each path's contribution in a mixed sample, each path needs to have a row vector $\boldsymbol{r}$, that contains typical spectrum shape caused by that path. $\boldsymbol{r}_{SingleBase}$

and $\mathbf{r}_{SingleDebris}$ can be used as single scattering component spectrum shape vectors without any conditioning. Vectors for paths with multiple scattering (here 1, 3, and 5) can be created with equation (32) from the single scattered components. Absolute values of these vectors have no significance so the variable *c´* in that equation can have any arbitrary constant value, e.g. c = 1. Scattering component matrix $\boldsymbol{A}$ can be generated with these component spectrum shape vectors.

$$\mathbf{A} = \begin{bmatrix} \mathbf{r}_{Path1} \\ \mathbf{r}_{Path2} \\ \dots \\ \mathbf{r}_{PathN} \end{bmatrix} = \begin{bmatrix} r_{Path1}(\lambda_1) & r_{Path1}(\lambda_2) & \dots & r_{Path1}(\lambda_M) \\ r_{Path2}(\lambda_1) & r_{Path2}(\lambda_2) & \dots & r_{Path2}(\lambda_M) \\ \dots & \dots & \dots & \dots \\ r_{PathN}(\lambda_1) & r_{PathN}(\lambda_2) & \dots & r_{PathN}(\lambda_M) \end{bmatrix} \tag{34}$$

Now if list of spectrum shapes is complete it can be stated that:

$$\boldsymbol{\gamma}_{Fit} \cdot \mathbf{A} = \mathbf{R}_{Fit} \approx \mathbf{R}_{Obs} \tag{35}$$

where $\boldsymbol{\gamma}$ is a row vector containing weight of each spectrum shape component listed earlier. If the scattering component matrix is invertible, then $\boldsymbol{\gamma}$ can simply be solved from equation (35):

$$\boldsymbol{\gamma}_{Fit} = \mathbf{R}_{Obs}\mathbf{A}^{-1} \tag{36}$$

where $\boldsymbol{A}^{-1}$ is [pseudo]inverse of matrix $\boldsymbol{A}$. Although if scattering component matrix does not contain all components needed in perfect fit or if measured spectrum is noisy then the received $\boldsymbol{\gamma}$ may contain negative values or be otherwise non-physical solution to the scattering problem. If this should be the case, there are a number of possible solutions for the problem:

- Remove noisy wavelengths from data in the fitting phase.
- Alter $\boldsymbol{A}$ to resemble more the real physical process.
- Average data to reduce noise. (Excess averaging also causes more error)

If all solutions above fail then the fitting of $\boldsymbol{\gamma}$ must be done some other way, E.g. by Monte Carlo approach where physical values for $\boldsymbol{\gamma}$ are generated and then tested in equation (35). Particularly in cases in that numerous components are searched for, this solution is substantially slower than any solution created with equation (36).

If an acceptable fit for $\boldsymbol{\gamma}$ is found, then the absolute reflectance spectrum caused by path *i* can be separated with:

$$\mathbf{r}_{Abs\ Route\ \ i} = \boldsymbol{\gamma}_i \mathbf{r}_{Route\ \ i} \tag{37}$$

4 Finnish Geodetic Institute Field Goniospectrometer (FiGIFiGo)

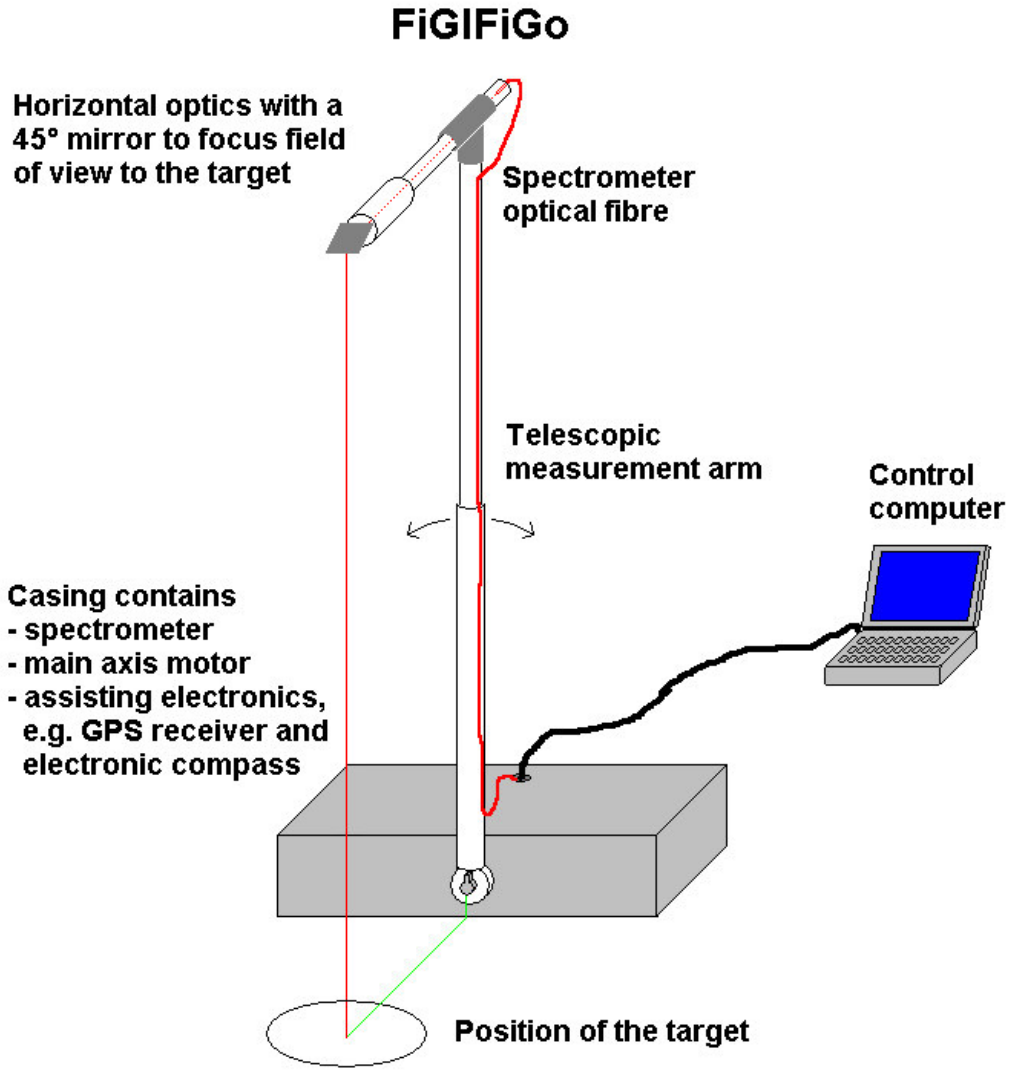

Figure 7. A diagrammatic drawing of FiGIFiGo. The measurement arm turns so that target can be observed from multiple zenith angles. The arm length can be selected between 150 and 270 cm. Total weight of the illustrated equipment is approximately 30 kg.

At Finnish Geodetic Institute we have developed an instrument for retrieval of Bidirectional Reflectance Factor (BRF). It is named as FiGIFiGo (Finnish Geodetic Institute Field Goniospectrometer). (Figure 7) It is an automatic, portable goniospectrometer that can be used to quickly and easily measure the spectral BRF (350-2500 nm) of small outdoor and indoor targets. By now FiGIFiGo has been used for BRF retrieval on multiple campaigns for e.g. various forest understorey species, snow, gravel, asphalt, sand, conifer shoots, and remote sensing tarps.

FiGIFiGo is weather proof and it is transportable even through rough terrain owing to its light weight of 30 - 50 kg (depending on configuration). FiGIFiGo can be further separated to smaller components and be reassembled again in 10 to 15 minutes. Measurement of one hemisphere takes 10 to 30 minutes. If BRF at multiple illumination zenith angles is required, then also multiple hemispherical measurements are needed. Measurements can be carried out either using the sunlight or a 1000W laboratory light source. FiGIFiGo can reach the zenith angles of up to 80 degrees in any azimuth direction and is self-shadowing only at area of 5-degree diameter around the exact backscattering direction.

FiGIFiGo is not a ready-made instrument and constantly under development as our measurement needs change over time. The instrument described in this thesis is the development version that was operational during summer 2006. While the measurements for this thesis have been made already by the end of year 2005, no controversial development have been done between these versions. During spring 2006 new measurement arm and custom-made optics with depolarizer were installed in to FiGIFiGo. The advantage of the new optics is that it removed an error source caused by polarization sensitivity of the spectrometer. However this error occurs still on the measurements of this thesis, and its effects are discussed more closely in chapter 5.

4.1 Operation

FiGIFiGo is basically a spectrometer that measures the spectrum of light reflected from target to multiple directions. Multiple zenith observation directions are achieved by positioning the target on the axis of turning measurement arm with spectrometer optics facing the target in the middle. (See Figure 8) Azimuth alteration is achieved by rotating the whole instrument around the target.

Figure 8. FiGIFiGo in operation. FiGIFiGo measures automatically the reflected spectrum from a series of beforehand-defined zenith angles. Typically measurements are done at zenith angles from –70° to +70° between 2.5° or 5° interval. Measurement of one such arch takes 60-120 seconds depending on the interval and integration time. The filmstrip was photographed in laboratory at METLA research station in Suonenjoki.

Basic measurement process in laboratory starts with equipment set-up. Everything is powered up and the control program in the computer is started. Direction of light source is defined and entered in to the program. By measuring Spectralon white reference standard from nadir direction the spectrometer integration times are optimized and calibrated. The to-be-measured target is positioned in the middle of goniometer and instrument is turned around the target to the wanted azimuth direction. Azimuth angle is either read from electronic compass of entered manually to the program. After this, with a single button operation the FiGIFiGo measures the reflectance from a pre-defined series of zenith angles over the target. Typically this is done from –70° to +70° with 2.5° or 5° interval. After 1-2 minutes FiGIFiGo has finished the arch and the device can be turned to another azimuth direction and a new arch is measured. 3 to 6 arches are usually considered to give sufficient description of BRF.

At field measurements with sunlight a few alterations in the measurement process are done.

1. Sun position is constantly calculated from GPS data. Light position definition is not needed, but it is handled automatically.
2. Measurement azimuth direction does not need to be entered manually but it is received automatically from an electronic compass if location is free of magnetic disturbance.
3. Because of sun movement and atmospheric disturbance the illumination does not stay constant. Thus before each arch spectrometer should be recalibrated with white reference standard.
4. To compensate with irradiance variance during an arch, the irradiance is constantly recorded with a pyranometer. This pyranometer value is used as a correction term in data processing. Pyranometer records also provide confidence over the stability of illumination by providing cloud detection.
5. In natural illumination, the diffuse light is always present. Thus at least once during the BRF retrieval the nadir reflectances from shaded target and shaded white reference standard should be measured. These reflectances are needed in data processing.

4.2 Technical

In this chapter technical aspects of FiGIFiGo are introduced. All major component devices are described. Electronics of FiGIFiGo system are mainly not custom made, but standard products by various manufacturers. On the other hand almost all mechanical components have been custom made. The mean power consumption is about 50 W. Input power can be provided between 11 and 18 volts, from which two additional voltage levels of 5 and 24 volts are transformed from.

4.2.1 ASD FieldSpec PRO FR – spectrometer

'Analytical Spectral Devices FieldSpec PRO Full Range'-spectrometer is FiGIFiGo's main sensor. It is a portable spectrometer with optics connected through 4 m optical fibre. It has spectral range from 350 - 2500 nm with output resolution of 1 nm. However true observation resolution is 3 nm at 700 nm, and 10 nm at 1400 and 2100 nm. [23.] The spectrometer is moderately rain, shock and dust proof. The measurements for this thesis were made with the original 3°, d = 11 mm, optics. Afterwards new improved 2″ custom-made optics were installed.

4.2.2 Thermo Oriel 1000W QTH laboratory light source

When sun is not used as illumination source the Quartz-Tungsten-Halogen (QTH) laboratory light source is used instead. Actual power usage can be altered with the power source. The maximum power is 1000W. Usage of artificial illumination source of course demands that the measurements are done either in laboratory or outside after the sunset.

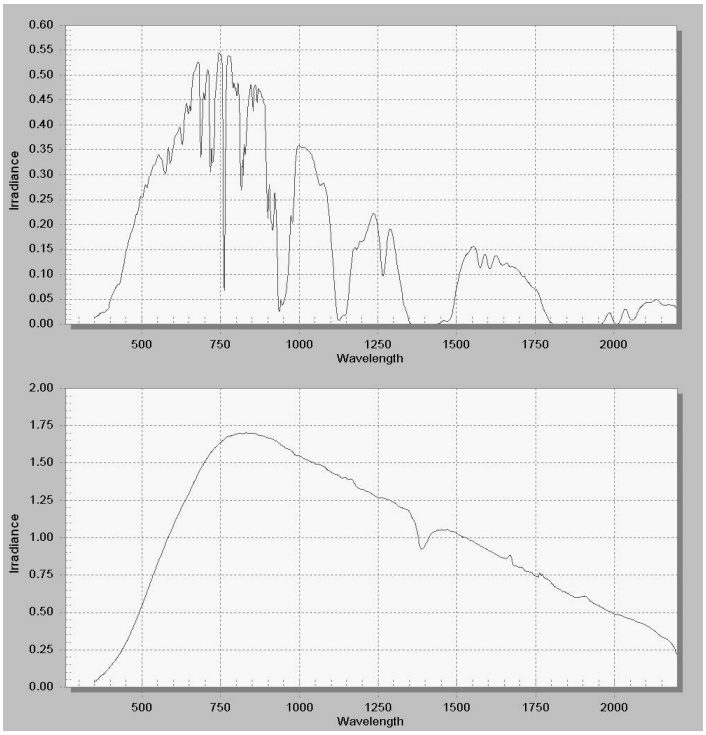

Figure 9. Spectral irradiances of sunlight (upper) and QTH lamp illumination (lower, operated with 900W power). Sun irradiance was measured at noon on a clear day in January in Masala, Finland. QTH illumination was measured from much closer than normally used in measurements. Thus the absolute irradiance values of sun and QTH should NOT be compared.

4.2.3 Panasonic Toughbook CF-18 rugged laptop

Toughbook CF-18 (see Appendix B) is the control computer in our measurement system. Toughbook has all the features of a modern laptop computer plus it can withstand practically all hazards normally met at fieldwork. It has 10.4" outdoor-readable colour LCD touchscreen. Toughbook is fully moisture and dust resistant and can withstand reasonable shocks. It is operational in temperatures as low as -20^{o}C. In another words Toughbook can be safely used without any special caution or protection in all possible environments in which measurements would be sensible.

4.2.4 Heavy laboratory base

Heavy steel laboratory base provides an easy and accurate mean to accomplish azimuth turn of instrument that is needed during the BRF retrieval. The base is actually the old base of the FGI goniospectrometer model 3. The steel base is such inmaneuverable that it is used only in our own laboratory.

4.2.5 Plywood base

Outside our laboratory a plywood base called “banana” is used for assistance in azimuth turn. This base is banana shaped and it is placed around the target. The banana has a rail that keeps FiGIFiGo at correct distance from target center. If extreme lightweight configuration is required, the BRF retrieval can also be made without base of any kind.

4.2.6 Hydrogen cell

When no wall outlet power supply is available, a hydrogen cell powers FiGIFiGo. Our hydrogen cell is model HC-100 by a Finnish company Oy HydroCell Ltd. HC-100 with 200-litre low-pressure metal hybrid storage weighs 3.7 kg and can give 1.6 A @ 12 V for approximately 25 hours without reload. Although this is not enough to fully power up the system it significantly prolongs the buffer battery life.

4.2.7 Kipp&Zonen SP-Lite pyranometer

Kipp&Zonen SP-Lite pyranometer (see Appendix C) is used for recording sunlight irradiance. SP-Lite is silicon-based pyranometer with its pros and cons. Silicon pyranometer has quick response to irradiance changes, and it is small and rugged. The spectral range is only from 400 nm to 1000 nm. Thus coverage over whole sunlight spectrum is not received. A thermocouple pyranometers would have wider spectral range, but their slow integration time make then unfit for cloud detection.

4.2.8 Haicom HI-204S GPS receiver

HI-204S is a small rugged USB-powered and -connected GPS receiver.

4.2.9 Internal organs

In addition to external components list above, FiGIFiGo contains also many inbuilt "invisible" components that have significant role in usability of instrumentation. In addition to fuses, diodes, various connectors, and a few meters of cable, the goniometer has inbuilt the following components:

- DC motor, gear box, and control logic by Faulhaber*
- LabJack U12 analog to digital converter card*
- VTI SCA-121 inclinometer*
- KVH C100 electronic compass*
- 12V 7.2 Ah lead buffer battery
- Vanson SDR-120W 12 to 24 V power transformer
- Custom-made 5 V regulator with heat sink.
- 7 port USB-hub with external power
- USB to RS-232 adapter
- Quatech PCMCIA to LPT-port adapter

The components marked with * in the above list are described more closely in next subchapters.

4.2.9.1 Faulhaber DC motor, gear box, and control logic

The heart of the goniometer is the Faulhaber 48 volt brushless DC-servomotor (4490 048 BS), which turns the measurement arm thru 352:1 gearbox. The motor is controlled with Faulhaber MCBL2805 motion controller. The controller is given stepper-motor-like commands through RS-232 serial port.

4.2.9.2 LabJack U12 analog to digital converter card

LabJack U12 is a compact USB connected measurement card. It is the connection point between all our analog output sensors and control software on laptop computer. LabJack has 8 single-ended or 4 differential 12-bit analog inputs with input range of ± 10 volts. LabJack U12 also has 2 analog outputs and 20 digital IO-ports.

4.2.9.3 VTI SCA 121T DO3 inclinometer

VTI SCA 121T DO3 (see Appendix D) is gravitation based dual axis analog output inclinometer. SCA121 is rugged, small, and it has capability to provide full angular range. Accuracy depends on analog to digital conversion and on tilt angle, but typically 1° repeatability is reached.

4.2.9.4 KVH C100 electronic compass

Electronic compass is used in field measurements to automatically detect the sensor azimuth angle. KVH C100 offers highest degree of accuracy available for portable electronic compasses. In typical circumstances the accuracy and repeatability of heading is better than one degree.

4.3 Software

FiGIFiGo's runtime software consists of two parts. (1) Gonio.vi is the main program that controls all operation of FiGIFiGo. (2) RS³ is the spectrometer control program provided by manufacturer. It is the only mean to control ASD spectrometers built before 2005 because no separate drivers are provided. Gonio.vi contains functions for software control of RS³ thru innovative keyboard emulation, ini-file manipulation, and watching over spectrum file creation. These functions are unique, and have raised interest worldwide by providing the only mean to control older ASD spectrometers with custom software.

FiGIFiGo does not produce directly a single file BRF but a log-file containing parameters of each spectrum measurement and hundreds of separate ASD spectrum-files. Data-processing software is needed for BRF retrieval from these raw data. I have written such functions for Matlab. Jouni Peltoniemi has developed similar functions with GUI for IDL.

4.3.1 Gonio.vi

Gonio.vi is the program that controls the whole measurement process. It is built on National Instruments LabView development environment. Gonio.vi enables the automation of measurement process and provides all essential controls and indicators on one screen. I have single-handedly written Gonio.vi.

4.3.1.1 LabView environment

LabView is a graphical development environment created to easily and flexibly build measurement system control programs. Even thought LabView is a product of a private company National Instruments, it has become "industrial standard" in measurement systems. Practically all major sensor and laboratory equipment developers provide LabView drivers for all instrumentation that is connected to a computer.

LabView is used in our solution mainly because it provides an easy graphical interface to follow the input data in real time. One of the benefits of LabView when compared to more traditional text based programming languages is that there is no need to compile the program before using it. If there is a problem with the code, the program points out the location of the bug and code can be altered instantly at measurement location.

4.3.1.2 Operation

Before the actual measurements some basic definitions about the measurement must be done in the Gonio.vi's initialization page. (Figure 10) On initialization phase log-file (.glg) is created and initialized, RS³ is started, and possibly GPS data is received.

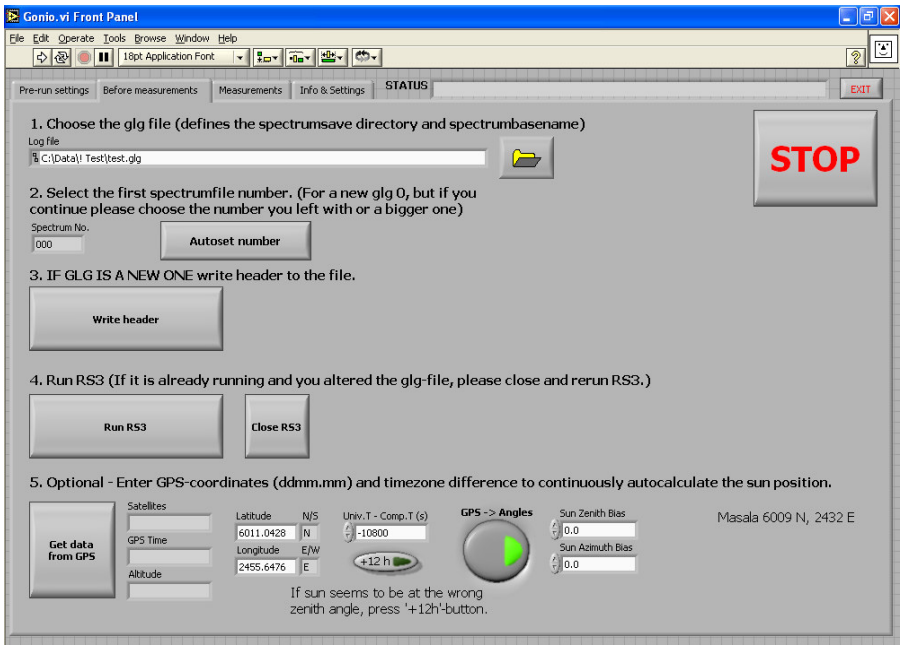

Figure 10. Initialization page of Gonio.vi.

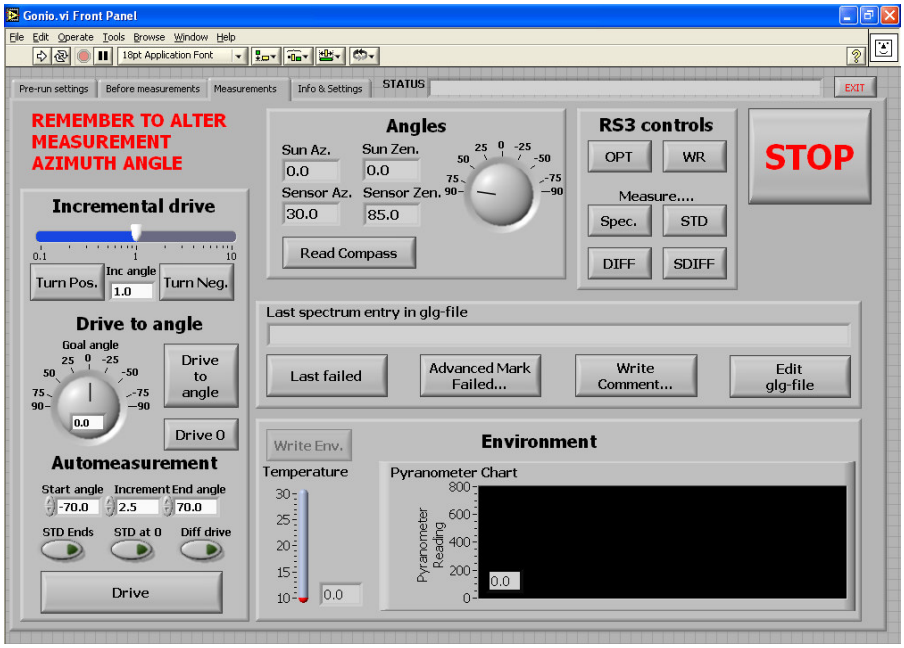

Figure 11. The main window of Gonio.vi. "Measurement"-page is used during the measurements and it contains all controls needed in basic measurements.

After the initialization is completed main page of Gonio.vi is opened. (Figure 11) It contains all the controls that are needed during BRF retrieval. Following functionalities are available

- Angles of illumination and observation can be entered and their current values are show.
- Arm position can be moved with incremental or absolute angle drive.
- Measurement drive executes spectrum measurements from a series of zenith angles defined by start angle, end angle, and increment.
- Spectrometer can be optimized, white reference target can be measured, and spectrums can be measured.
- Comments can be added to the log file.
- Last spectrums can be marked as failed if something went wrong with measurement
- Pyranometer value history is shown for easy cloud detection
- Emergency stop button operation is always enabled.

An entry is written in the log file basically always when Gonio.vi makes an action. The beginning of the log file contains basic information about the measurement, i.e. target description, date, time, location, light source, measurer, and weather description. Spectrum line in log file contains name of the spectrum file, target name, angles of illumination and observation, pyranometer value while the spectrum was measured, and time.

4.3.2 RS^3

RS^3 (see Figure 12) is the control software for spectrometers manufactured by Advanced Spectral Devices inc such as our ASD FieldSpec Pro. RS^3 takes care of all operations needed to use spectrometer. Some of the most used features are optimization, calibration, dark current measurement, and spectrum save.

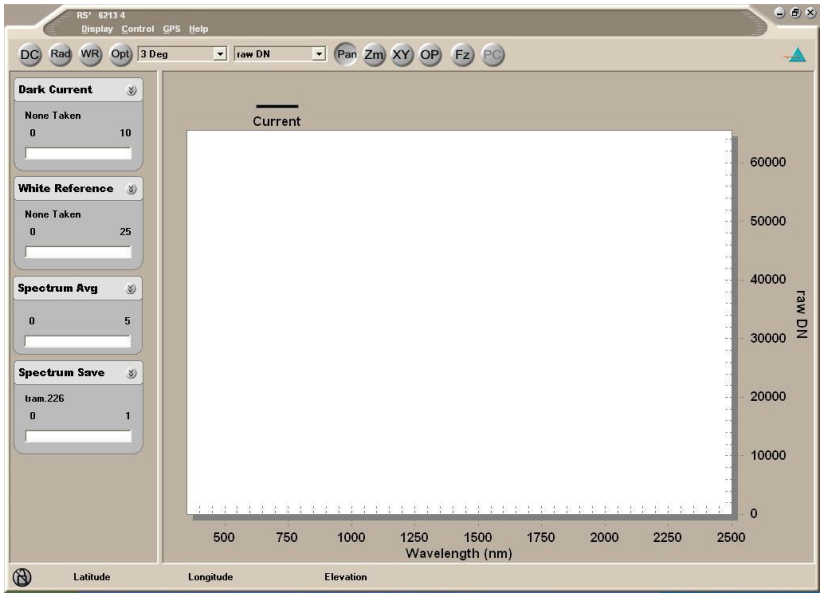

Figure 12. RS ³ main window. RS ³ is the spectrometer control program provided by ASD and it is the only way to control older LPT version of spectrometer

There is no other way to control old ASD spectrometer than to do it through RS^3. No external drivers exist. Unfortunately RS^3 does not support passing commands between programs thus allowing spectrometer to be controlled by another program, but all spectrometer commands must be transmitted through keyboard emulation.

4.3.3 Data processing software

Using the information from measurement's log-file the post-processing software collects data from ASD spectrum files and interprets these raw data to BRF. Read and visualisation codes exist for both Matlab and IDL. Also a real time LabView software to be used during measurements is under development.

4.4 Error source analysis

Due to complicated nature of the different measurement setups, exact error analysis that would produce simple error margins for measured reflectance factors is more than troublesome. Errors are produced by numerous separate sources:

- Error in reflectance sensors
    - Error from spectrometer
        - Thermal noise in spectrometer sensors.
        - Calibration may contain error if the white reference sheet is not exactly levelled or it is misplaced. The sheet may also be dirty.
        - Spectrometer optics may be dirty and thus produce error.
        - The optics does not observe only collimated light, but collects light from a range of angles. Thus actual measurement is not directional, but conical. Because the opening angle of the optics and the distance-to-optics-size relation are small, it can usually be approximated that the observation is directional. However there is a source of error in this.
    - Thermal noise in pyranometer.
- Noise in definition of observation angles
    - Zenith angle is defined with an inclinometer
        - The inclinometer is based on measurement of acceleration. Movement and vibration of the sensor causes error.
        - The inclinometer measures and outputs the sine of zenith angle. Accuracy after the AD-conversion depends heavily on the zenith angle.
    - Azimuth angle is usually defined with the electronic compass.
        - Any steel or other magnetic substance too close causes (invisible!) error.
        - Compass calibration alters with location. (magnetic north vs. true north) Poor calibration leads to systematic error.

- Observed target is not constant …
  - … spatially.
    - An inhomogeneous target is not represented adequately by too small sample area.
    - Various reasons (listed below) may cause the observed area to alter during measurement. For inhomogeneous targets this has unpredictable influence in data. Practically all natural targets are inhomogeneous!
  - … over wavelength.
    - Optics work differently for different wavelengths (different refraction index). Thus observed area varies too.
    - The spectrometer contains three separate sensors for different wavelength ranges. Each sensor uses only it's own part of the optical fibre bundle. If focused optics is used, each sensor observes slightly different area.
  - … over observation angle.
    - An oval area is observed from tilted observation angles (on a flat surface). Oval area differs from the round nadir observation area and it cannot be kept constant over azimuth rotation.
    - Centre of observation can be held constant only at one height. This may cause problems with 3D-structured targets.
    - Imperfect alignment of the instrument and optics result to "wandering" of the centre of observation area.
    - Targets may not be rotationally symmetric. E.g. leaves are often pointing south. Thus the usual approximation that only relative azimuth angle has effect may not be correct. Horizontal movement of the sun may cause trouble.
  - … over time.
    - Sensitive targets, e.g. snow, may corrupt or metamorphosis during measurement.
    - Transportation of target to laboratory may alter its properties.

- Incident illumination is not constant
    - The sun moves constantly. Especially zenith movement causes alteration in irradiance.
    - Atmospheric effects
        - Greatest variation occurs usually on the wavelengths, on which water vapour absorption occurs. Spectrally affective clouds may be invisible to bare human eye.
        - Full cloud shadows are quite easy to detect. Thus they mostly are only nuisance. However clouds passing near the sun also change irradiance, because of their high tendency to forward scattering.
        - Amount and position of clouds affects intensity and directional distribution diffuse light.
    - The intensity of irradiation decreases relative to $1/r^2$, where r is the distance between the light source and the target. With sun this can be ignored, but with lamp only a few meter away this causes significant spatial variation in irradiance. Also problems with calibration may occur.
- Human effects
    - Mistakes in the measurement process
    - Full or partial shadows over target and pyranometer
    - Bugs in control program should not exist, but they tend to cause trouble and unexpected errors in system under development.

Due to the vast length of the previous list it is practically impossible to deduce exact error margins for a real BRF measurements by only implementing the error propagation law. A great portion of the previously listed errors tackle with the problem that the target alters between the measured points and wavelengths. Once again if the target is homogeneous and large enough this does not cause any trouble. Also the effect of the error in observation angles depends on the target. E.g. If the target is an ideal Lambertian surface, the error in observation angles has no effect at all. By this means the resulting error in BRF depends always on the targets properties and thus error margins cannot be universally solved.

However it is possible to yield error margins for some of the subcomponents of the data.

Subcomponent	**Error**
Sensor zenith angle	
- at nadir	$\Delta\theta_o = \pm 1°$
- at 45°	$\Delta\theta_o = \pm 2°$
Sensor azimuth angle	
- using compass (no magnetic interference)	$\Delta\phi_o = \pm 2°$
- manually by using a foundation with scale	$\Delta\phi_o = \pm 3°$
Light source direction	
- GPS & sun position algorithm	$\Delta\theta_i = \pm 0.1°$
	$\Delta\phi_i = \pm 0.1°$
- Manual definition	$\Delta\theta_i = \pm 2°$
	$\Delta\phi_i = \pm 2°$
Noise in reflectance factor	
(Spectralon from nadir, λ = 450 - 950 nm)	
- using sunlight on a clear day	$\lvert\Delta R\rvert < 0.01$
- using sunlight on a mediocre day	$\lvert\Delta R\rvert < 0.05$
- using lamp in laboratory	$\lvert\Delta R\rvert < 0.01$
Movement of the centre of observation	*Radius of*
(nadir view, azimuth rotation 360°)	*a circle*
- At laboratory, with steel base	*r = 2 cm*
- At field, level terrain, flat target	*r = 5 cm*
- At field, rough terrain, complex target	*r = 10 cm*
Movement of the centre of observation	*Movement*
(zenith turn –70° to +70°)	
- a flat target, good positioning	$\Delta x = \pm 10$ *cm*
- At field, complex target, tricky position	$\Delta x = \pm 25$ *cm*

Table 1. Typical errors in a BRF measurement with FiGIFiGo.

Also the application of measured data usually requires for more processing to be done. Illumination and observation geometry of interest is often not exactly same as in goniospectrometer measurement. An interpolation can be done, if geometry of interest fits inside the measured point cloud. If this is not possible or not preferred to be done, a BRF-model must be fitted. If geometry of interest fits closely enough the measurements this end processing may reduce error. But on the other hand extrapolation can also often be a significant error source.

The errors from many of these sources could still be reduced with additional sensors, sturdier structures, enhanced sample preparation, etc. However this is not always sensible task to do because FiGIFiGo is meant to be a portable goniospectrometer for measurement of natural targets. Important words there being “portable” and “natural targets”. Firstly expansions on the instrument would directly lead to more weight and lesser portability. Secondly 1% accuracy is not usually even needed with natural targets. The variation within one sample species is far greater than that. Time of year, time of day, last week’s weather, moisture, soil type, amount of shadow during whole day, competition, density of the growth. These all, and many other things, have a significant effect on what e.g. blueberry bush looks like. While majority of these variations cannot be mapped and recorded, it is not sensible to trade portability for excess accuracy.

5 EXPERIMENT

5.1 Measurements

The goal of these experiments was to find out how BRF of a flat natural boreal forest understory changes when more and more natural debris covers it. However in this experiment synthetic targets were used instead in laboratory illumination so that experiment could be controlled more precisely and unwanted alteration of target would be minimal.

5.1.1 Samples

A grey canvas was used as the base on which a well-defined amount of wooden cocktail toothpicks were randomly scattered on. The canvas was same material as is used in Finnish Geodetic Institutes "Siemens-star" aerial photography calibration target. [24.] The cocktailpicks were ordinary wooden cocktail toothpicks that are available in almost every grocery store. They were 68 mm long cylinders that narrow towards both ends with centre diameter of about 2 mm. 1000 cocktailpicks weighed 125 grams.

In the first experiments plain, bright cocktailpicks were used. For the second series of experiment darker cocktailpicks were manufactured by dyeing plain ones with coffee and concentrated blackcurrant juice. After an over-weekend-soaking cocktailpicks were dried in approximately 70°C oven. The goal of dyeing was to achieve geometrically identical target with lower single scattering albedo. However the dyeing process caused some swelling in cocktailpicks. If geometrically exactly similar targets would have been needed, then also bright cocktailpicks could have been soaked in water and dried in similar fashion. Effects caused by dyeing and increased surface roughness are discussed in chapter 5.3.1.

In both experiments canvas was spread out flat in laboratory. A carefully weighed amount of cocktailpicks were scattered evenly in random posture over a fixed area on the canvas. (Figure 13) Principal plane reflectances were measured with artificial illumination at 50^{o} zenith angle. Samples with 0, 12, 25, 38, 50, 75, 100, 225, and 350 grams of debris were measured with both bright and dark cocktailpicks.

Figure 13. Nadir photographs of samples with 12 (top left), 25, 50, 75, 100, and 225 (bottom right) grams of bright cocktailpicks scattered over area.

5.2 Data Processing

5.2.1 Pre-conditioning of data

The measurements were made between approximately 2.5 degrees so to ease comparison and to enable various mathematical procedures the data was interpolated over zenith angle with step of 1 degree. The laser pointer that helps in the localisation of spectrometer footprint disturbs the measurements at wavelength of 650 nm. Thus data was also interpolated between 625 nm and 675 nm. Because sharp wavelength depending effects were neither expected nor discovered the data was averaged over ± 10 nm interval in order to smooth noise.

The error caused by the shadow of the sensor in exact backscattering direction was NOT cut off or treated anyway special. This causes all the processed data to have no reliability at this exact backscattering direction and close around it. Due to this all results between –40 and –60 degrees should be inspected critically i.e. hot spot related results cannot be obtained from this data.

It was found out some time after these measurements that the ASD spectrometer is sensitive to polarization of the measured light. However the reflected light is often polarized because of the reflection processes. Thus steps in spectrum (see Figure 14) can often be seen at the sensor limits (approximately at 1000 nm and 1800 nm). This error seems to occur especially with both SWIR sensors, but not so strongly on the VNIR sensor (350 - 1000 nm). Afterwards we have fixed this problem by using custom-made optics with a depolarizer. However because the depolarizer was not yet in use with these measurements, the steps made it unreliable to use reflectance over sensor limits. Thus only VNIR sensor data is used.

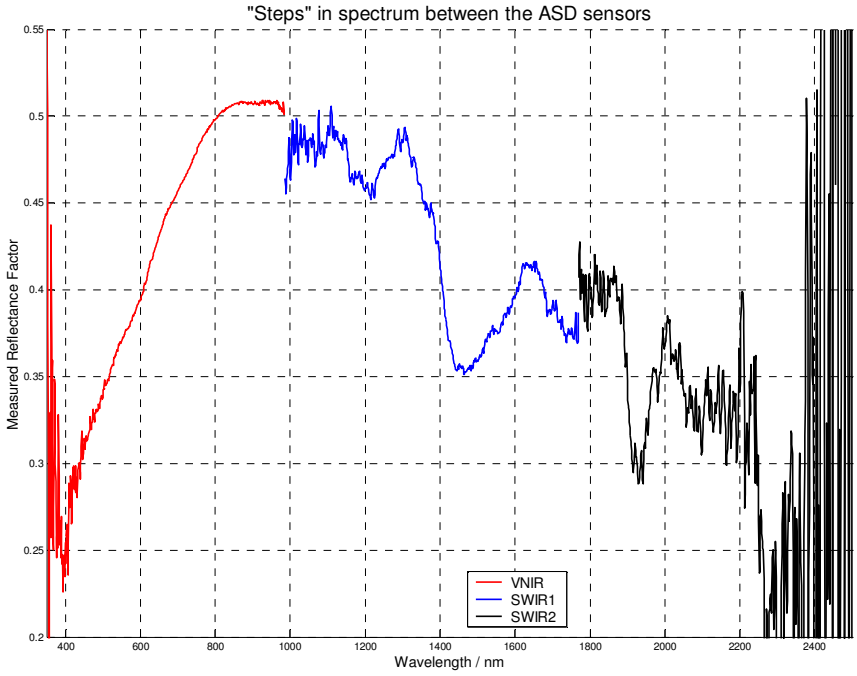

Figure 14. Steps in spectrum can be seen between the different sensors of ASD FieldSpec Pro spectrometer. Separate sensors (VNIR. SWIR1, and SWIR2) are marked with colours. The steps are mainly caused by polarization sensitivities of the sensors.

5.2.2 Scattering path separation

Data were organized to reflectance spectrum row vectors $\boldsymbol{R}_{\theta,d}$, which were built for each integer zenith angle and each amount of debris:

$$\mathbf{R}_{\theta,d} = \left[R_d(\theta,\lambda_1), \quad R_d(\theta,\lambda_2), \quad \ldots \quad R_d(\theta,\lambda_n)\right] \tag{38}$$

where θ is the principal plane zenith angle and d is the amount of debris.

The principal plane reflectances for both pure base (m_{debris} = 0 g) and pure debris (m_{debris} = 350 g) were measured at the principal plane. The single scattered components were separated from these by using the method described in chapter 3.4. The used outbound scattering probabilities for debris and base were heuristically set to 0.50 and 0.55 respectively. Heuristic method was found out to be adequate because slight alteration of these values didn't seem to have phenomenal effects on results.

In separation of scattering paths various different significant path combinations were tried. The best fit for data was found with an assumption that the significant scattering paths were following:

1. A few scatterings from base but none from debris
2. Single scattering from base
3. Single scattering from both base and debris
4. Single scattering from debris
5. A few scatterings from debris but none from base

where 3. was formed with equation (32); and 1. and 5. were respectively:

$$\begin{aligned} \mathbf{r}_{MultiBase} &= \mathbf{R}_{PureBase} - \mathbf{r}_{SingleBase} \\ \mathbf{r}_{MultiDebris} &= \mathbf{R}_{PureDebris} - \mathbf{r}_{SingleDebris} \end{aligned} \tag{39}$$

The spectrum component matrix $\boldsymbol{A}$ was created similarly as in chapter 3.4.3, but the simple fitting of $\boldsymbol{\gamma}$ refused to produce a physical solution despite numerous alterations. Fitting was forced to do the hard way i.e. with iterative variation of $\boldsymbol{\gamma}$. Following limits were set for values of $\boldsymbol{\gamma}$ to keep the solution physical:

$$\begin{aligned} &\gamma_i \geq 0, \quad \forall i \\ &\gamma_1 \leq 1.1 \cdot \gamma_2 \\ &\gamma_5 \leq 1.1 \cdot \gamma_4 \end{aligned} \tag{40}$$

Firstly negative values were banned because negative $\boldsymbol{\gamma}$ would lead to negative reflectance. The two latter limitations mean basically that the amount of multiple scattering from a component should be at its maximum in a pure sample of that component. The fitted $\boldsymbol{\gamma}$ seemed to produce with equation (37) a logical set of separated reflectance spectrums.

The fit was found to be quite precise. The mean deviation between the measured and fitted values was only 0.0025 (0.54 %) with the samples with light cocktail picks, and 0.0039 (1.33 %) with dyed cocktail picks. Some samples of the data and fitted model can be seen in Figure 15 and Figure 16.

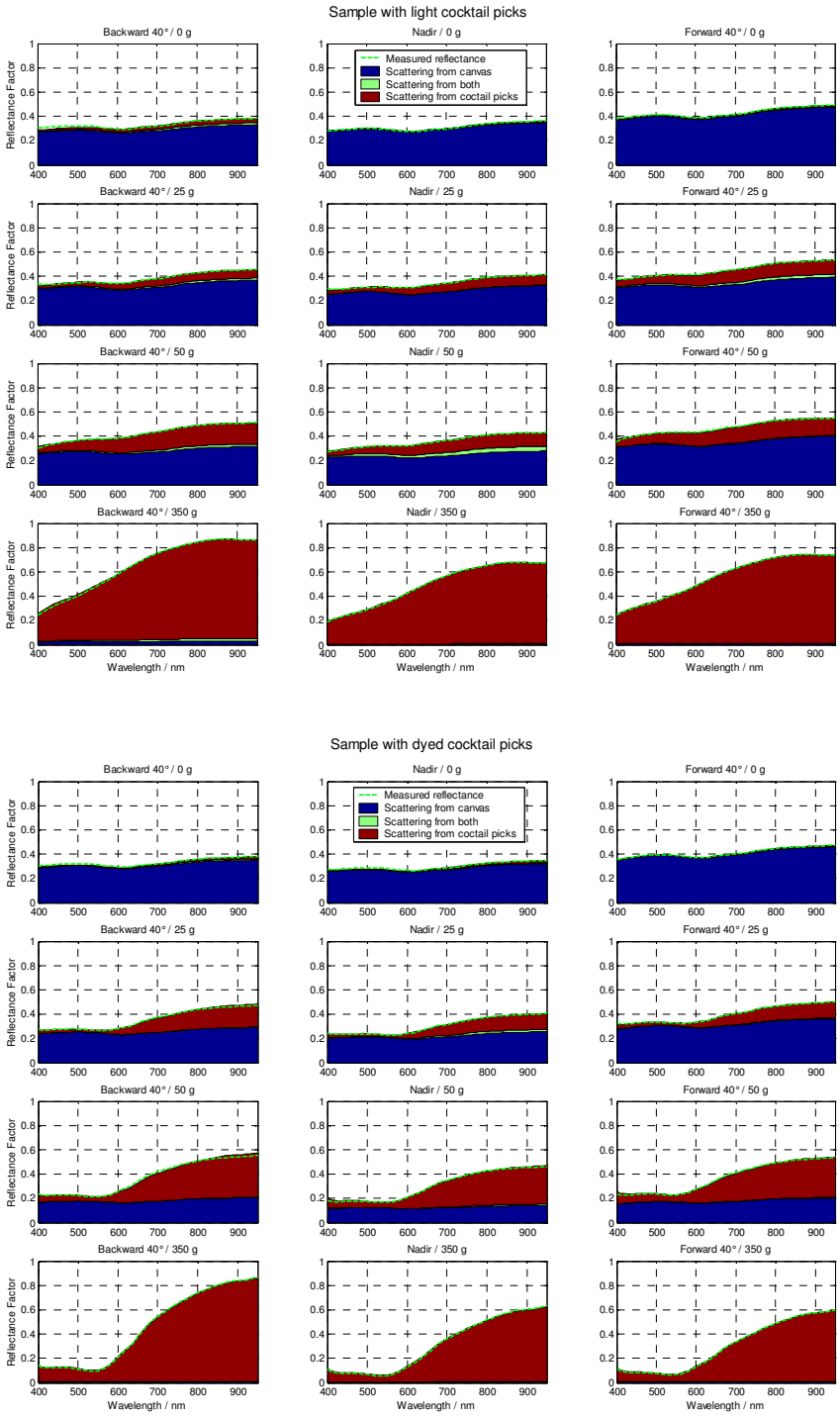

Figure 15. (light cocktail picks) and

Figure 16. (dyed cocktail picks) The model presented in this thesis was fitted to the measured reflectance data. The spectra were separated mathematically to components that have interacted with canvas and cocktail picks. The quality of fit can be evaluated by examining correlation of measured spectra (green line) and the top edges of the coloured areas.

5.3 Results

In the first experiments plain, bright cocktailpicks were used. For the second series of experiment darker cocktailpicks were manufactured by dyeing plain ones with coffee and concentrated blackcurrant juice. Natural dyes were used in order to maintain the increase in reflectance at near infrared region, that is typical for nearly all organic materials. As it can be seen from Figure 17 the dyeing affected the spectrum mostly only on wavelengths shorter than 1000 nm.

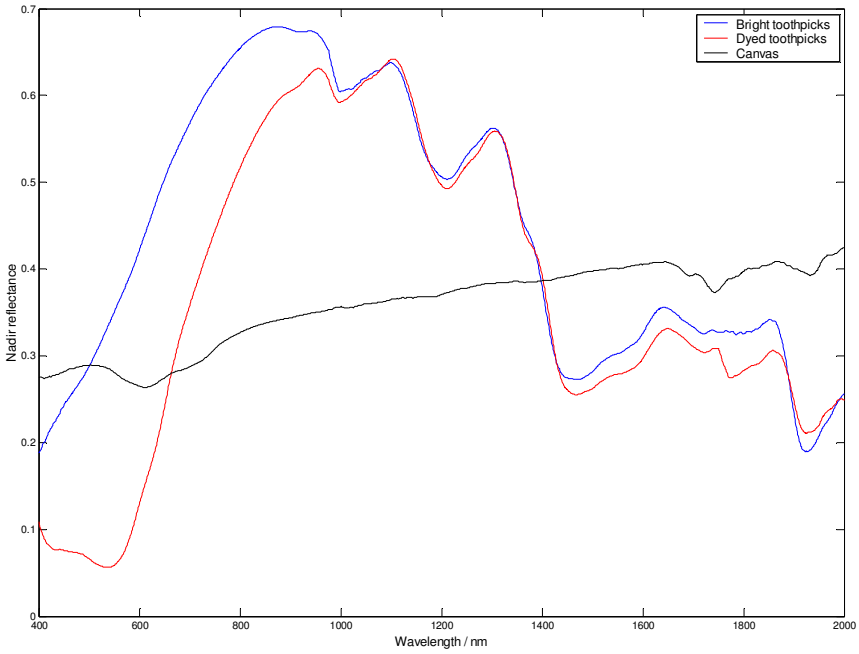

Figure 17. Nadir reflectances of pure samples. Each measured sample consisted of the base canvas (black line) and varying amount of cocktailpicks of one type (blue and red).

5.3.1 Effect of cocktail pick surface roughness

The dyeing process caused some swelling in cocktail picks. The diameter of unconditioned cocktail picks was 1.88 ± 0.06 mm, while dyed ones had swollen to 2.12 ± 0.08 mm. The wood fibres in cocktailpicks had loosened from original smooth surface. (Figure 18) This can be easily verified by sliding a finger back and forth against cocktailpick. Plain ones feel smooth both ways, while dyed ones feel considerably rougher when slided against the direction of fibres.

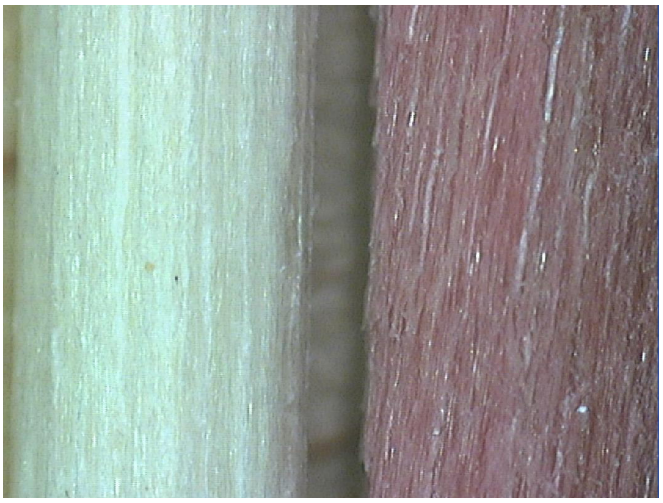

Figure 18. A microscope image of bright and dyed cocktailpick. The dyed cocktailpick has swollen in course of dyeing process and has significantly rougher surface than the bright one has. The image is approximately 4 mm wide.

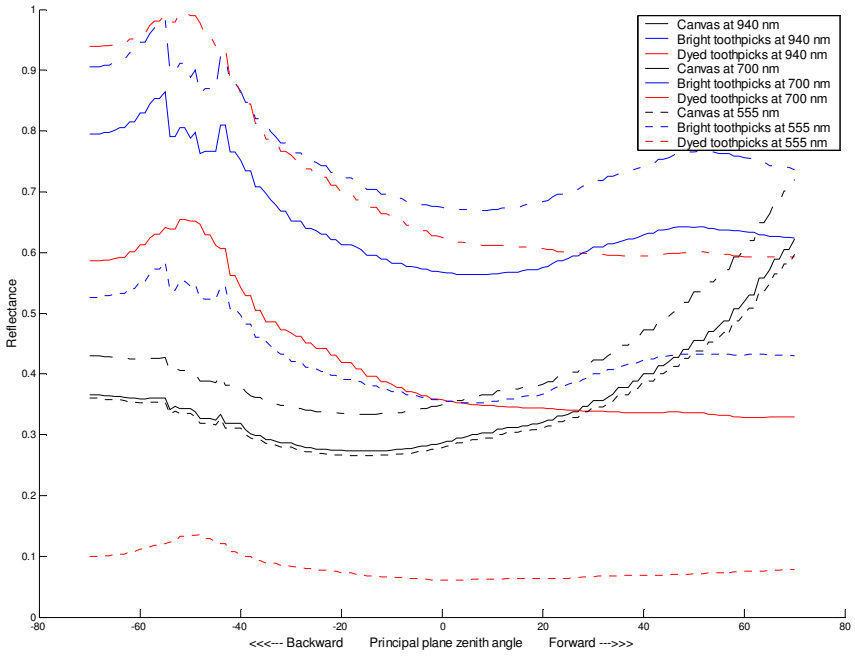

Figure 19. Principal plane reflectances of pure sample components. It is noteworthy how strongly dyeing process has decreased forward scattering. It can be seen clearly by comparing samples light and dyed samples with approximately same single scattering albedo on different wavelengths. E.g. by comparing dyed picks at 700 nm (solid red line) with bright picks at 555 nm (dotted blue line) or bycomparing their values at 940 nm.

In Figure 19 it can been seen that backscattering has increased and forward scattering has decreased due to dyeing. BRF of the dyed cocktailpicks has lost the concave shape that is typical for the BRF of plain ones.

The two samples differ basically in two ways: (1) Dyed cocktailpicks are darker i.e. their single scattering albedo is lower. (2) Due to rougher surface scattering phase function of the dyed picks emphasizes more backward scattering. This is because rough surface decreases the cocktailpicks' tendency for mirror-kind specular reflection.

5.3.2 The effect of packing style

In the first series of measurements with light cocktail picks, the effect of packing density was experimented. First 50 grams of cocktail picks were scattered evenly over the canvas in random postures. Principal plane reflectances for this sample were measured. For the second measurement the same cocktailpicks were shuffled so that they were set in slightly more organized fashion i.e. packing density was increased. For human eye the most noticeable thing was that more cocktailpicks were parallel to each other.

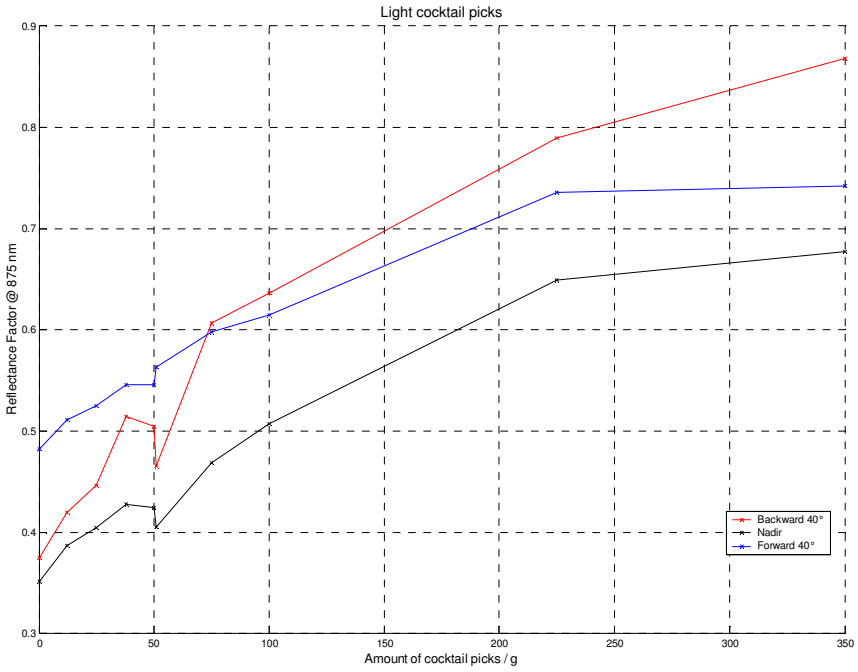

Figure 20. The measured reflectance factor at 875 nm as function of amount of light cocktail picks. The reflectance factor follows vaguely exponential behaviour. The step at x = 50 g is caused by the shuffling of cocktail picks. At x = 50 g the picks are still at their original randomly dropped positions. At x = 51 g the picks are shuffled to more regular posture. The effect of this shuffling seems to disappear quite quickly when more random picks are added to the top.

The change in cocktail pick postures did produce a distinct variation in BRF. (Figure 20.) The forward scattering was increased during shuffling, because the levelling of

the picks created more horizontal surfaces that endorse specular reflection. The drop in reflectance to the other directions is probably the outcome of the same effect. If more light is scattered to forward direction, less light there is left to be scattered to the other directions. Also due to more even distribution, the cocktail picks could cover the underlying canvas more efficiently. Thus the portion of reflectance from cocktail picks was slightly increased. (Figure 21.)

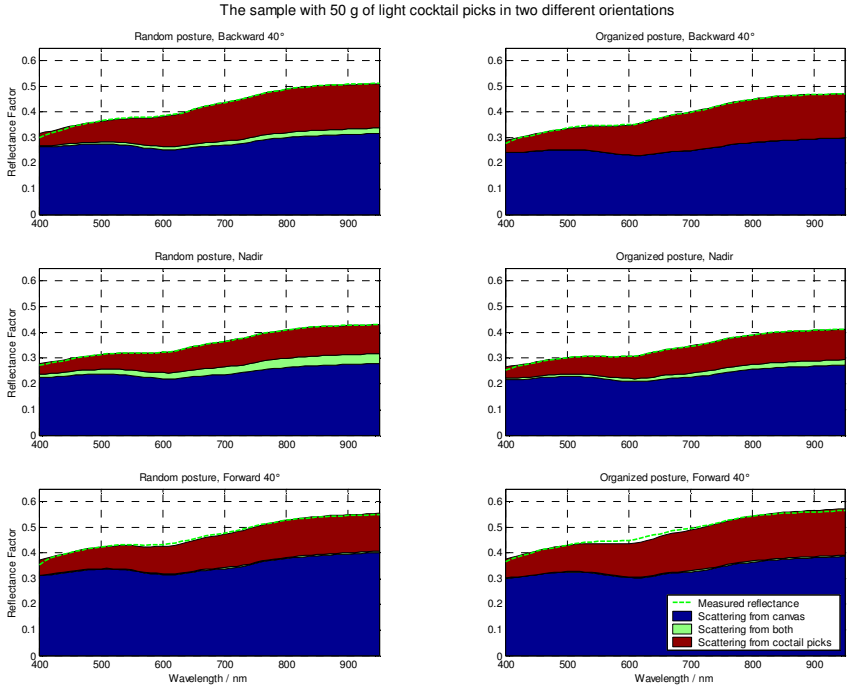

Figure 21. The effect of packing density on a sample. The sample was first measured with the cocktail picks dropped in a random posture (plots on left). For the second measurement the sample was shuffled so that cocktail picks were more parallel to each other.

Figure 20 and Figure 22 are showing the measured reflectance factors as function of amount of cocktail picks. Both graphs show vaguely inverted exponential behaviour. This is expected because when more picks are covering the canvas, then each new pick has lesser probability to cover the canvas and greater probability to cover earlier picks. This kind of process leads naturally to inverted exponential shape.

Figure 22 shows also interesting behaviour at large amounts of cocktail picks. The reflectance factor drops significantly for the nadir and forward directions, but stays near constant for the backward scattering. This is probably caused by a change in the picks' postures. When there is only a thin layer of cocktail picks, all picks are set more or less horizontally. However a thicker layer allows some of the picks to stay also in more vertical stances and thus amount of shadows is increased. Amount of shadows does not play a significant role in backscattering due to shadow hiding, while nadir and forward scattering are affected.

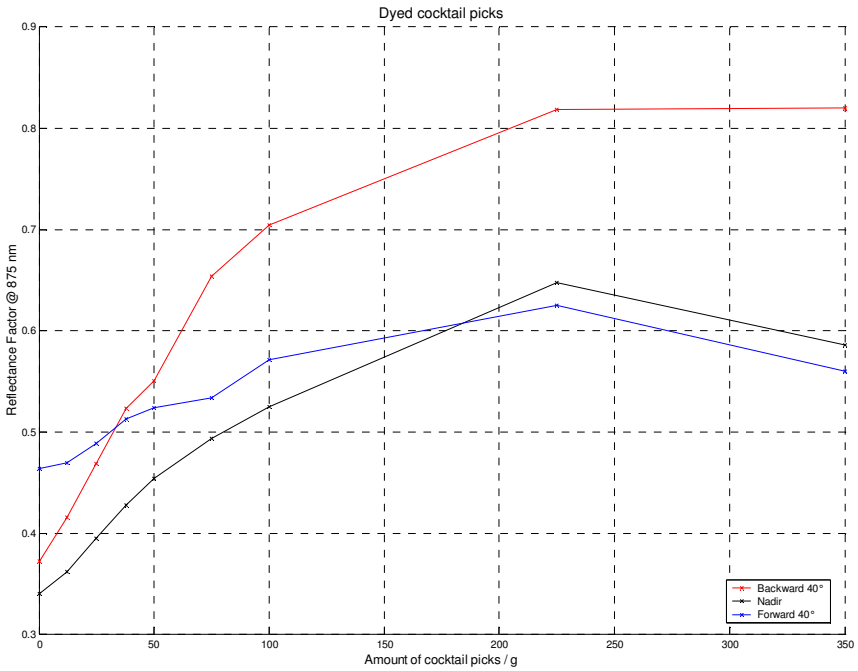

Figure 22. The measured reflectance factor at 875 nm as function of amount of dyed cocktail picks. The reflectance factor follows vaguely exponential behaviour until 225 g, but when still more picks are added the nadir and forward scattering curves drop.

6 CONCLUDING DISCUSSION

6.1 A brief summary

Finnish Geodetic Institute Field Goniospectrometer (FiGIFiGo) is an instrument developed for Bidirectional Reflectance Factor (BRF) retrieval of small, relatively homogenous targets e.g. forest understorey or asphalt. FiGIFiGo is a portable device that is operated by 1 or 2 persons. It can be reassembled to a new location in 15 minutes and after that a target can be measured in 10 – 30 minutes (with one illumination angle). FiGIFiGo has effective spectral range approximately from 400 nm to 2000 nm. The measurements can be made either outside with sunlight or in laboratory with 1000 W QTH light source. A diffuse light correction allows retrieval of BRF also in natural hemispherical sunlight illumination.

A new method was introduced for extraction of subcomponent proportions from reflectance of a mixture sample, e.g. for retrieving proportion of lingonberry in reflectance of lingonberry-lichen sample. This method was tested by conducting a series of measurements on reflectance properties of mixture samples. Artificial samples were manufactured by placing exact amounts of cocktail toothpicks in random postures on a grey canvas. Both natural wooden cocktail picks and geometrically identical dyed ones were used.

6.2 Conclusions

FiGIFiGo has now reached such technical maturity that it can be said to be fully operational device. It can be reliably used for quick and easy BRF retrieval. Although still more improvements are planned, most of them are not crucial for the instrument operation.

During the development work and use of FiGIFiGo it has come clear that portability is an important feature in a goniospectrometer. During the last two years and especially during our latest campaign in August 2006 we have been able to measure targets with FiGIFiGo that would be unreachable for most of the other similar devices. For example in Abisko, Sweden, we measured dwarf birch bushes on the top of a mountain that was reachable only with a light cable car. Also BRF of a lake was measurements from a small boat. Also the speed of measurement process has been found to be crucial. On perfectly clear day measurements can be made any speed, but on partly cloudy days a fast operation is needed. For effective campaign use measurements must be possible also on imperfect days. Often measurement needs occur quite rapidly. Thus it is also handy that only two persons are needed for instrument assembly and operation.

But the FiGIFiGo measurement process is not yet perfect. Even lighter equipment with faster operation would be useful, variation in target pointing during measurement still causes some trouble and larger observed area on the sample would be needed with inhomogeneous targets. Also automation of spectrometer calibration would ease the use considerably. Despite these minor defects, to my knowledge, FiGIFiGo is the world's most functional and adaptive field goniospectrometer and definitely best suited for our needs. It would be useful if a larger research team would be working with FiGIFiGo due to the fact that now the instrument is not in use most of the time. The research work around FiGIFiGo could easily employ one or more modellers, physicists, physics oriented biologists, and laboratory engineers.

The component separation method produced sound results when applied to the data, but further verification of the method is still needed to be done. This method could be a valuable research tool in analysis of mixed samples and help in development of further reflectance models. However its direct capabilities in remote sensing use are limited due to the need of exact knowledge of the components.

Interesting observations of reflectance properties of mixture samples were made. With these limited measurements only simple conclusions can be made, but a larger data set is needed for deeper analysis of their reasons and recurrences. Thus more similar and expanded experiments are needed. Especially the effect of packing style on reflectance properties should be surveyed more, because it seems to have a significant effect on the results. This is a relevant problem especially for the study of vegetation targets, because they are most often packed in very special ways that are hard to define mathematically. Thus an effort should be made especially for finding the relevant parameters in packing style.

6.3 Plans for future

Development of FiGIFiGo will still continue. The new optics still requires some fine-tuning. A second optics tube with capability for polarized measurements will be manufactured. Also some improvements to target pointing accuracy are planned. The pyranometer might be replaced with a small spectrometer so that spectral information could be used for a better "pyranometer" correction. This new irradiance spectrometer could also reduce the frequency that white reference calibration is needed during measurements.

In addition to these mechanical improvements also our BRF data storage systems needs revising. Currently the data is stored in measurement format. This makes the old data hard to use because the format that it is stored in is altered by the development version of the instrumentation. Also finding all data that is relevant for a specific use is hard because of lack of indexing. Thus a new BRF database system is needed. When database is ready and operational it will be opened for scientific community through a Internet portal. Thus also an effective distribution format would be needed. In wider use such database could be used in new remote sensing applications and as a basis of new reflectance models.

FiGIFiGo will definitely be used frequently for a number of uses:

- Forest understorey research will be continued with one focus on mixture samples.
- During wintertime snow measurements will be made.
- FiGIFiGo will be used for ground reference measurements with FGI related aerial photography flights.
- Our BRF database will be expanded with all targets measured with FiGIFiGo.

During August 2006 a measurement campaign with Finnish Meteorological Institute was carried through in Sodankylä. Reference measurements were made with a spectrometer with 17-meter field of view over inhomogeneous ground. All subcomponents of this sample were measured. Thus it will now be possible to test the component separation method also with this data set.

The increasing number of goniospectrometers such as FiGIFiGo will increase our understanding of reflectance of our environment. However the physics of light reflectance in our environment is so complex that there will always be more mysteries left to be discovered.

7 REFERENCES

[1.] "**Special issue on MERIS"**, *International Journal of Remote Sensing, Volume 20, No. 9, 1999*

[2.] D. J. Diner, B. H. Braswell, R. Davies, N. Gobron, J. Hu, Y. Jin, R. A. Kahn, Y. Knyazikhin, N. Loeb, J.-P. Muller, A. W. Nolin, B. Pinty, C. B. Schaaf, G. Seiz, and J. Stroeve (2005) "**The value of multiangle measurements for retrieving structurally and radiatively consistent properties of clouds, aerosols, and surfaces**", *Remote Sensing of Environment, 97, 495-518*

[3.] B. Pinty, J.-L. Widlowski, M. Taberner, N. Gobron, M. M. Verstraete, M. Disney, F. Gascon, J.-P. Gastellu, L. Jiang, A. Kuusk, P. Lewis, X. Li, W. Ni-Meister, T. Nilson, P. North, W. Qin, L. Su, S. Tang, R. Thompson, W. Verhoef, H. Wang, J. Wang, G. Yan, and H. Zang (2004) "**Radiation Transfer Model Intercomparison (RAMI) exercise: Results from the second phase**", *Journal of Geophysical Research, 109, D06210*

[4.] *Glossary of Meteorology*, American Meteorology Society, Boston, MA, USA, 2000 (available also at http://amsglossary.allenpress.com/glossary)

[5.] M. Schönermark, B. Geiger, H. P. Röser, (2004) "**Reflection Properties of Vegetation and Soil**", *Wissenschaft und Technik Verlag, Berlin, Germany*

[6.] Hapke, B. (1993). "**Theory of reflectance and emittance spectroscopy**" *Cambridge University Press*

[7.] Natural Resources Canada - Centre for Remote Sensing, "**Glossary of remote sensing terms**", http://ccrs.nrcan.gc.ca/glossary/index_e.php (10.4.2006)

[8.] G. Schaepman-Strub, M. E. Schaepman, T. H. Painter, S. Dangel, J. V. Martonchik (2006) "**Reflectance quantities in optical remote sensing—definitions and case studies**", *Remote Sensing of Environment 103 (2006) 27–42*

[9.] S. Dangel, M. M. Verstraete, J. Schopfer, M. Kneubühler, M. Schaepman, and K. I. Itten (2005) "**Toward a Direct Comparison of Field and Laboratory Goniometer Measurements**", *IEEE Trans. Geosci. Remote Sens.*, vol. 43, no. 11, pp. 2666–2674.

[10.] Subfigures in Figure 1 were downloaded from Internet 10.2.2006.
Subfigure A: http://www.geo.unizh.ch/rsl/research/SpectroLab/goniometry/brdf_intro.shtml
Subfigure B: http://www.geo.unizh.ch/rsl/research/SpectroLab/radiometry/gonio_index.shtml
Subfigure C: http://ikb.weihenstephan.de/en/research/tp_5/actions.html
Subfigure D: http://syseng.arc.nasa.gov/syseng/pdf/AMS_Symposium_Paper.pdf
Subfigure E: http://landval.gsfc.nasa.gov/prove/grass/prove.html

[11.] C. Koechler, , B. Hosgood, G. Andreoli, G. Schmuck, J. Verdebout, A. Pegoraro, J. Hill, W. Mehl, D. Roberts and M. Smith (1994) "**The European Optical Goniometric Facility - Technical Description and First Experiments on Spectral Unmixing**", *Proceedings of IGARSS'94*, Pasadena, 8-12 August, 2275–2377

[12.] S. Sandmeier and K. I. Itten (1999) "**A Field Goniometer System (FIGOS) for Acquisition of Hyperspectral BRDF Data**" *IEEE Trans. Geosci Remote Sensing*, 37(2), 978–986.

[13.] S. Sandmeier (2000) "**Acquisition of Bidirectional Reflectance Factor Data with Field Goniometers**", *Remote Sens. Environ.* 73, 257–269

[14.] S. Schill and J. Jensen (2000) "**Modeling Bidirectional Reflectance Distribution Function (BRDF) of Smooth Cordgrass (Spartina**

Alterniflora) Using a Sandmeier Field Goniometer", *ASPRS 2000 Annual Conference Proceedings*, 178–184, Washington DC.

[15.] I. Manakos, T. Schneider, (2001) "**Field spectroscopic measurements for the approximation of the BRDF in the frame of precision farming**". *Proceedings of International Workshop on Spectroscopy Application in Precision Farming*, 68–73, Freising-Weihenstephan.

[16.] Bruegge, C. J., M. C. Helmlinger, J. E. Conel, B. J. Gaitley, and W. A. Abdou, (2000) "**PARABOLA III: A sphere-scanning radiometer for field determination of surface anisotropic reflectance functions**", *Remote Sensing Reviews*, Vol 19, 75–94.

[17.] T. H. Painter, B. Paden, J. Dozier, (2003) "**Automated spectro-goniometer: A spherical robot for the field measurement of the directional reflectance of snow**", *Review Of Scientific Instruments, 74, 12, 5179 - 5188*

[18.] J. I. Peltoniemi, S. Kaasalainen, J. Näränen, M. Rautiainen, P. Stenberg, H. Smolander, S. Smolander, and P. Voipio, (2005) "**BRDF measurement of understory vegetation in pine forests: dwarf shrubs, lichen, and moss**", *Remote Sensing of Environment,* 94, 343–354

[19.] J. I. Peltoniemi, S. Kaasalainen, J. Näränen, L. Matikainen, and J. Piironen (2005) "**Measurement of Directional and Spectral Signatures of Light Reflectance by Snow**", *IEEE Trans. Geosci Remote Sensing*, 43, 10, 2294–2304

[20.] B. Hapke, D. DiMucci, R. Nelson, and W. Smythe (1996) "**The Cause of the Hot Spot in Vegetation Canopies and Soils: Shadow-Hiding Versus Coherent Backscatter**", *Remote Sensing of Environment,* 58, 63–68

[21.] J. M. Suomalainen and J. Peltoniemi, (2006) "**Light Scattering Properties of Debris Covered Surfaces: Separating Components of Multiangular Reflectance**", *Proceedings of the XL Annual Conference of the Finnish Physical Society, March 9-11, 2006, Tampere, Finland*

[22.] G. M. Foody and D. P. Cox, "**Sub-pixel land cover composition estimation using a linear mixture model and fuzzy membership functions**", *Int. J. Remote Sensing, vol. 15, pp. 619-631, 1994*

[23.] D. C. Hatchell, (1999) "**ASD Technical Guide**", *4th ed., Analytical Spectral Devices, Inc., Boulder, CO, USA*

[24.] E. Honkavaara, J. Peltoniemi, E. Ahokas, R. Kuittinen, J. Hyyppä, J. Jaakkola, H. Kaartinen, L. Markelin, K. Nurminen, and J. Suomalainen, (Out 2007) "**A permanent test field for digital photogrammetric systems"** *Photogrammetric Engineering & Remote Sensing, Accepted.*

Appendices

Appendix A. Spectralon datasheet

Appendix B. Toughbook 18 specification sheet

Appendix C. Kipp&Zonen SP-Lite silicon pyranometer datasheet

Appendix D. VTI SCA 121 T DO3 datasheet